Mass Functions of the Active Black Holes in Distant Quasars from the Large Bright Quasar Survey, the Bright Quasar Survey, and the Color-Selected Sample of the SDSS Fall Equatorial Stripe

Vestergaard, Marianne; Osmer, Patrick S.

Published in:
Astrophysical Journal

DOI:
10.1088/0004-637X/699/1/800

Publication date:
2009

Accepted by The Astrophysical Journal, April 18, 2009
Preprint typeset using LaTeX style emulateapj v. 10/09/06

MASS FUNCTIONS OF THE ACTIVE BLACK HOLES IN DISTANT QUASARS FROM THE LARGE BRIGHT QUASAR SURVEY, THE BRIGHT QUASAR SURVEY, AND THE COLOR-SELECTED SAMPLE OF THE SDSS FALL EQUATORIAL STRIPE.

M. Vestergaard[1] and Patrick S. Osmer[2]

Accepted by The Astrophysical Journal, April 18, 2009

ABSTRACT

We present mass functions of distant actively accreting supermassive black holes residing in luminous quasars discovered in the Large Bright Quasar Survey (LBQS), the Bright Quasar Survey (BQS), and the Fall Equatorial Stripe of the Sloan Digital Sky Survey (SDSS). The quasars cover a wide range of redshifts from the local universe to $z = 5$ and were subject to different selection criteria and flux density limits. This makes these samples complementary and can help us gain additional insight on the true underlying black hole mass distribution free from selection effects and mass estimation errors through future studies. By comparing these quasar samples, we see evidence that the active black hole population at redshift four is somewhat different than that at lower redshifts, including that in the nearby universe. In particular, there is a sharp increase in the space density of the detected active black holes ($M_{\rm BH} \gtrsim 10^8 M_\odot$) between redshifts $\sim$4 and $\sim$2.5. Also, the mass function of the SDSS quasars at $3.6 \leq z \leq 5$ has a somewhat flatter high mass-end slope of $\beta = -1.75 \pm 0.56$, compared to the mass functions based on quasars below z of 3 (BQS and LBQS quasars), which display typical slopes of $\beta \approx -3.3$; the latter are consistent with the mass functions at similar redshifts based on the SDSS Data Release 3 quasar catalog presented by Vestergaard et al. We see clear evidence of cosmic downsizing in the comoving space density distribution of active black holes in the LBQS sample alone. In forthcoming papers, further analysis, comparison, and discussion of these mass functions will be made with other existing black hole mass functions, notably that based on the SDSS DR3 quasar catalog. We present the relationships used to estimate the black hole mass based on the Mg II emission line; the relations are calibrated to the Hβ and C IV relations by means of several thousand high quality SDSS spectra. Mass estimates of the individual black holes of these samples are also presented.

Subject headings: cosmology: observations – galaxies: active – galaxies: luminosity function, mass function – quasars: emission lines – quasars: general – surveys

1. INTRODUCTION

Black hole demographics has become a common and important ingredient of cosmological studies in recent years. One reason is the indication that black holes and their activity play a crucial role in the formation and evolution of galaxies (e.g., Granato et al. 2004; Springel, Di Matteo, & Hernquist 2005; Somerville et al. 2008) and galaxy clusters (e.g., McNamara & Nulsen 2007). To fully understand the impact of black holes on mass structures and their evolution we need to understand much better how they form, grow, and interact with their surroundings. A first step toward this goal is to take inventory of the population of supermassive black holes across the history of the universe. Unfortunately, it is not possible to study supermassive black holes in all types of galaxies with the same (mass estimation) method (e.g., cf. Magorrian et al. 1998; Vestergaard 2004b, 2009; Peterson et al. 2004), due to the varying physical conditions of their host galaxies, the varying activity level of the black holes themselves, and the large range of physical distances to the black hole host galaxies. Due to their faintness and the small angular extent of the central region that needs to be studied, quiescent or weakly active black holes can typically not be well studied beyond the local neighborhood of a few hundred Mpc (e.g., Ferrarese 2003). Since actively accreting black holes power the luminous quasars that are observable across the universe (e.g., Fan 2006), quasars offers a convenient way to trace the black hole population in the distant universe. The goal is that the combination of studies of active black holes with empirical and theoretical insight on the relationship between active and quiescent black holes and between obscured and unobscured black holes will eventually lead to realistic representations of the true and complete black hole population.

We can study the population of actively accreting supermassive black holes by studying the large catalogs of quasars and active galaxies obtained through the numerous large, extensive quasar and AGN UV and optical surveys that have been made since the discovery of quasars [e.g., The multi-color survey of stellar objects by Koo & Kron (1982), Palomar-Green Survey (Schmidt & Green 1983), UK-Schmidt Telescope Survey (e.g., Kibblewhite et al. 1984; Hewett et al. 2001), Canada-France-Hawaii Telescope Survey (Crampton, Cowley, & Hartwick 1987), CfA Redshift Survey (Huchra & Burg 1992), Palomar Transit Grism Survey (Schmidt, Schneider, & Gunn 1995), 2-degree-field survey (2dF; Smith et al. 2005), and Sloan Digital Sky Survey (SDSS; York et al. 2000)]. No-

Electronic address: m.vestergaard@tufts.edu, osmer.1@osu.edu
[1] Dept. of Physics and Astronomy, Robinson Hall, Tufts University, Medford, MA 02155
[2] Graduate School and Department of Astronomy, The Ohio State University, 230 N. Oval Mall, Columbus, OH, 43210

tably, any survey with its own set of selection criteria will tend to preferentially select either for or against objects with particular spectral or broad band properties. Therefore, by studying only quasars studied by a single selection method there is a risk that we may limit ourselves to only part of the actual underlying black hole population. We aim to minimize this potential issue by including in our ongoing study of the black hole population and the black hole mass functions several quasar samples. The current work focuses on the mass functions based on the following samples: the Bright Quasar Survey (BQS; e.g., Schmidt & Green 1983), the Large Bright Quasar Survey (LBQS; e.g., Hewett, Foltz, & Chaffee 1995), and the color-selected sample from the Fall Equatorial Stripe (Fan et al. 2001a) of the SDSS.

The BQS, LBQS, and the SDSS color-selected samples are each based on different selection criteria, namely UV excess, spectral shape on objective prism plates, and broad-band colors, respectively. Especially, the BQS and the LBQS are each complementary to the SDSS DR3 quasar selection (Richards et al. 2002). For example, the SDSS selection probability decreases significantly for quasars at redshifts of about 2.8 to 3.2 because the colors of quasars at these redshifts coincide with the stellar locus in the selected color spaces (Richards et al. 2006). This limits the usefulness of the DR3 quasar black hole mass function (Vestergaard et al. 2008) at and near this redshift range which is particularly important since this is the epoch at which the quasar space density peaks (e.g., Osmer 1982; Warren, Hewett, & Osmer 1994; Schmidt et al. 1995; Fan et al. 2001a, 2001b). The different selection criterion of the LBQS can instead help shed light on the mass distribution at the affected redshift range, especially given the large size of this quasar sample (1067 quasars) and its wide redshift range. The favorable properties of the somewhat smaller BQS sample are that it is selected over a very large sky area (10700 square degrees) and includes the brightest quasars in the nearby universe. Therefore, the BQS is suitable for anchoring the bright end of the luminosity function and the high mass end of the black hole mass function in the nearby universe. Also, the colors of the BQS quasars are not typical of SDSS quasars (Jester et al. 2005) and the BQS thus makes a different contribution to our insight on black hole mass distribution than the SDSS alone can provide. The value of the SDSS color-selected sample studied here is that it is a well-defined, complete (to within the color-selection criteria, the survey area, and the flux density limits) and homogeneous quasar sample at redshift $3.6 \leq z \leq 5.0$ that is highly suitable for statistical studies. This redshift range is beyond that of the LBQS ($z \leq 3.0$ for the mass functions) and is where the number statistics of the SDSS DR3 mass function quasar sample is lower. The availability of a well-defined selection function for this color-selected sample (Fan et al. 2001a) therefore gives us an excellent opportunity to determine the black hole mass function for a homogeneous and well-defined sample at high redshift which thus renders an additional opportunity for constraining the black hole mass distribution at earlier epochs.

The added values of the samples studied here are that luminosity functions have been determined for both the LBQS (e.g., Boyle et al. 2000) and the SDSS color-selected samples (Fan et al. 2001a). Potentially, by combining the luminosity and black hole mass functions for the same quasar samples we can break the degeneracies (related in part to the unknown mass dependency of the radiative efficiency and mass accretion rate) that limit the use of the luminosity functions alone (e.g., Wyithe & Radmanabhan 2006). By combining the three quasar samples studied here with the SDSS DR3 quasar sample for which the luminosity and mass functions have already been determined (Richards et al. 2006; Vestergaard et al. 2008) we anticipate to gain a better understanding of the true underlying black hole mass distribution than is possible by studying either of these samples alone.

In this work we present the black hole mass functions of the BQS, LBQS, and the SDSS color-selected quasar samples which collectively cover the entire redshift range up to $z = 5$ and contain nearly 1200 sources. We adopt the most recently calibrated mass scaling relations utilizing broad line widths and continuum luminosities (i.e., Vestergaard & Peterson 2006; Vestergaard et al. 2008 and references therein) in cases where the more robust reverberation mapping mass determinations (Peterson et al. 2004) are not available. Although the mass estimates based on scaling relations are less robust than the reverberation mapping masses and are potentially prone to systematic uncertainties (e.g., Krolik 2001; Richards et al. 2002; Vestergaard 2004a, 2004b, 2009) they perform surprisingly well considering the circumstances (e.g., Vestergaard 2004b, 2009; Vestergaard & Peterson 2006; Marconi et al. 2008). In fact, there is suggestive evidence based on Hβ data that scaling relations can be improved to yield mass estimates that are within a factor 1.6 (or 0.2 dex) of the reverberation masses when radiation pressure on the broad line gas is taken into account (Marconi et al. 2008). This uncertainty rivals the scatter of the quiescent black holes in the $M_{\rm BH}-\sigma$ relationship ($0.25 - 0.3$ dex; Tremaine et al. 2002).

Source inclination is known to affect the velocity dispersion of the broad line region as measured using the widths of broad optical and UV emission lines (e.g., Wills & Browne 1986; Vestergaard, Wilkes, & Barthel 2000). In fact, source inclination is expected to be one of the factors that account for at least part of the scatter in the $M_{\rm BH}$ values around the $M_{\rm BH}-\sigma$ relationship (although the inclination is not trivially connected to object location relative to the $M_{\rm BH}-\sigma$ relationship; e.g., Collin et al. 2006) and which at present limits the accuracy of mass determinations of active black holes to some degree. Considerations have also been made on the relative usefulness of the various line widths (e.g., the line dispersion versus the FWHM width) (e.g., Peterson et al. 2004; Denney et al. 2008) and a correction scheme was suggested (Collin et al. 2006) to correct mass estimates based on FWHM measurements of Hβ to mass estimates based on the line dispersion values which are preferred for the high-quality reverberation mapping database (Peterson et al. 2004). Unfortunately, for neither of these effects (radiation pressure, inclination, and the potential inadequacies of the FWHM parameter) are the influences on our determination of black hole masses understood or parametrized well enough that corrections can be applied to our mass estimates for all three emission lines, Hβ, Mg II, and C IV, used here. Also, for this study we need our entire data base to be coherent and homogeneously analyzed and all mass estimates to be based on similar

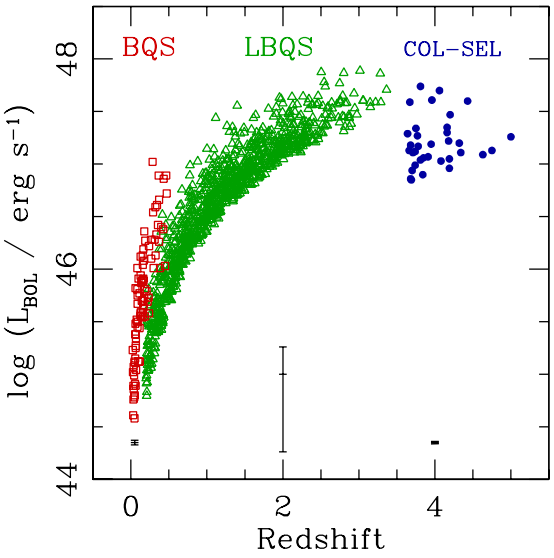

FIG. 1.— Distributions of bolometric luminosities, $L_{\rm bol}$, as a function of redshift for the LBQS (triangles), BQS (squares), and SDSS color-Selected (filled circles) samples. Typical measurement errors are shown in the lower portion of the diagram. For the LBQS the $L_{\rm bol}$ values are based on the survey B_J magnitudes, causing large errors due to the necessary extrapolation across the spectrum.

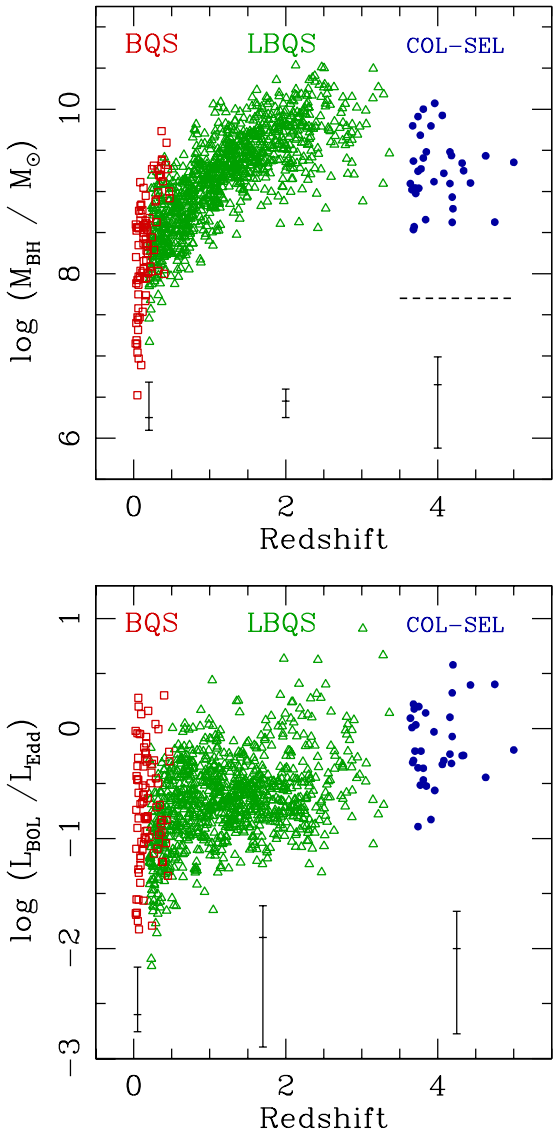

FIG. 2.— Distributions of black hole mass, $M_{\rm BH}$, (top panel) and Eddington luminosity ratios, $L_{\rm bol}/L_{\rm Edd}$, (bottom panel) as a function of redshift for the LBQS, BQS, and SDSS color-Selected samples. Symbols are as in Figure 1. The dashed line in the top panel shows the SDSS flux density limit folded with the line width cut-off of 1000 km s^{-1} adopted for SDSS quasars. See the discussion for details.

assumptions. For these reasons, we make no attempt to correct the mass estimates at this time.

The mass functions presented here will be analyzed further in relation to the black hole mass functions of the SDSS DR3 quasar sample (Vestergaard et al. 2008) for the purpose of extracting the true underlying mass distribution using the statistical methods introduced and discussed for the luminosity function by Kelly, Fan, & Vestergaard (2008a) and for the mass function by Kelly, Vestergaard & Fan (2009). If, at that time, we are capable of making corrections for any of the effects outlined earlier such that the mass estimates or the associated error distribution change significantly, the mass functions will be updated accordingly.

A cosmology of $\rm H_0 = 70$ km s^{-1}Mpc^{-1}, $\Omega_\Lambda = 0.7$, and $\Omega_m = 0.3$ is used throughout.

2. DATA

The three quasar samples for which we determine the black hole mass functions are summarized in the following sections, in order of their redshift coverage. As outlined in section 3, the black hole mass estimates are based on measurements of the widths of the Hβ, Mg II, and C IV profiles and nuclear continuum luminosities. These spectral measurements are therefore also summarized in the following.

2.1. *The Bright Quasar Survey*

The Bright Quasar Survey (BQS; Schmidt & Green 1983) is a subset of the quasars discovered in the Palomar-Green Survey of UV excess sources ($U - B < -0.46$; Green, Schmidt, & Liebert 1986) undertaken in 1973 − 1974 using the 18 inch Palomar Schmidt telescope with classification spectroscopy obtained with the Hale 5 m telescope. This survey was done using photographic B_J plates that were later digitized. It has an impressive area coverage of 10714 deg^2 and a flux limit of about $B_J \approx 16.1$ mag. Here, we include the 87 objects at $z \leq 0.5$ for which Boroson & Green (1992) present spectroscopic data. We use the spectral measurements (i.e., line widths and continuum luminosities) adopted by Vestergaard & Peterson (2006) where the details of the data are also described.

The mass distribution of the BQS sample was previously studied by Vestergaard (2004a). Since that work, the mass scaling relationships have been updated owing to improvements made to the reverberation mapping database (Peterson et al. 2004). Therefore, for the few BQS quasars for which robust black hole mass measurements have been obtained using reverberation mapping (Peterson et al. 2004), we adopt these mass determinations in our analysis with exception of PG2130+099 for which the mass has recently been further improved (Grier et al. 2008). For the remaining sources we adopt the

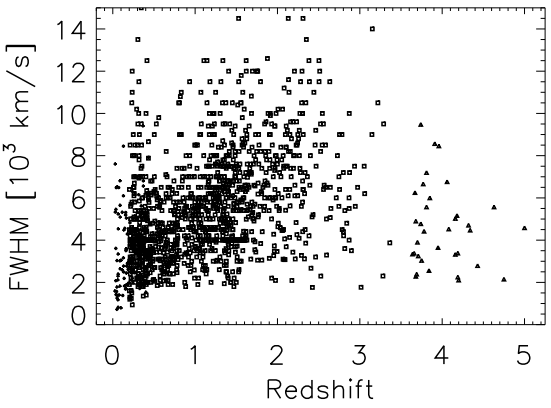

FIG. 3.— Distributions of line widths (FWHM) as a function of redshift for the LBQS (squares), BQS (asterics), and SDSS color-Selected (triangles) samples. No significant changes are seen in the distribution with redshift, except the SDSS color selected sample does not have as extreme wide lines as some LBQS quasars.

mass estimates based on the most recently updated mass scaling relationships. These mass values are listed in Table 7 of Vestergaard & Peterson (2006).

2.2. *The Large Bright Quasar Survey*

The Large Bright Quasar Survey (LBQS; e.g., Foltz et al. 1987; Hewett et al. 2001) is the largest published spectroscopic survey of optically selected quasars at bright ($B_J < 19$ mag) apparent magnitudes as of 1995. It consists of 1067 quasars located at redshifts between 0.2 and 3.4 and it covers an effective area of 453.8 deg^2 on the sky. The quasar candidates were selected from the Automated Plate Measuring machine scans of the United Kingdom Schmidt Telescope direct and objective-prism plates based on their spectral energy distribution shapes on these plates. The details of the survey are published in a series of papers and most recently summarized by Hewett et al. (2001) who also present an updated account of the survey completeness as a function of redshift.

Spectroscopic observations were obtained in the late 1980's at a resolution of $6 - 10$ Å using the 4.5 m Multi Mirror Telescope (MMT) with a wavelength range of $\lambda\lambda 3300 - 7500$ Å or with the Las Campanas 2.5 m Du Pont Telescope with a wavelength range of $\lambda\lambda 3400 - 7000$ Å (Morris et al. 1991). In these configurations the Hβ, Mg II, and C IV emission lines are observed in the spectra of quasars at redshifts between 0.2 to about 0.4 − 0.5, between 0.2 to 1.5 − 1.65, and between 1.2 − 1.26 to a redshift of about 3.4, respectively. The presence of two different spectral wavelength ranges should not affect our results since each spectrum will contain at least one of the Hβ, Mg II, and C IV emission lines for the redshift range from 0.2 to 3.0.

Forster et al. (2001) performed automated spectral modeling of the LBQS spectra and, in particular, present line width measurements for 993 of the 1067 quasars of the full LBQS sample. The remaining quasars were not modeled because of strong broad and narrow absorption in the Ly α and C IV emission lines. The spectra were modeled with a powerlaw continuum component, UV and optical Fe II emission templates (Vestergaard & Wilkes 2001; Boroson & Green 1992), and Gaussian emission and absorption line functions. Most of the broad emission lines were modeled with a single Gaussian profile from which the FWHM was obtained. A small fraction of the spectra are of high enough quality to allow two Gaussian functions to be fitted to the lines. For the single Gaussian models we adopted the measurements of the FWHM and uncertainties tabulated by Forster et al. (their Table 5). To determine the FWHM of the emission lines modeled with multiple Gaussian components we first regenerated the modeled line profile from the tabulated model parameters of all the components. Then we measured the FWHM of the regenerated profile (i.e., as the full width at the half maximum peak value). The measurement uncertainties of the FWHM in this case were obtained by a suitable weighting of the uncertainties in the tabulated measurements of the individual Gaussian components. These weights were estimated as the weights to be applied to the FWHM measurements of the individual Gaussian components so to obtain the FWHM of the sum of the components (determined from the regenerated line profile, described above). For each of the broad emission lines (Hβ, Mg II, C IV) a separate weight was determined. We note that only a few quasars had emission lines modeled with multiple Gaussian components: 7 Hβ, 118 Mg II, and 79 C IV lines, respectively (out of a total of 148 Hβ, 677 Mg II, and 488 C IV profiles, respectively). For profiles for which Forster et al. fixed the line width (no uncertainties were estimated) we adopt a typical measurement error of 10% (e.g., Brotherton 1996).

Because the LBQS spectra are not flux calibrated, we determined the nuclear monochromatic continuum luminosities not from the spectra but from the survey B_J magnitudes.

Given the modest quality of the spectra we visually inspected the spectra of quasars with FWHM measurements listed by Forster et al. to be either below 2000 km s^{-1} or above 12,000 km s^{-1}. The reason is that very small and very large line widths measurements are more prone to be spurious in spectra of modest quality and they can significantly affect the mass functions owing to the relatively smaller number of such extreme objects. The fact that the Forster et al. profile measurements above 12,000 km s^{-1} tend to have large uncertainties confirm our general suspicion. Most of the very broad line profile fits of Forster et al. are typically listed for profiles of quite poor quality (with a few having strong absorption in addition); in a couple of cases, the fitting must have gone bad. We found all C IV profiles with FWHM $\geq$ 17,000 km s^{-1} had to be discarded for these reasons and a few profiles of about 12,500 − 14,000 km s^{-1} have too noisy profiles to be useful. In addition, most of the Mg II FWHM measurements listed to be above 12,000 km s^{-1} are based on very noisy, unreliable data; these measurements were discarded from further analysis. For the profiles listed to have FWHM $\lesssim$ 2000 km s^{-1}, we find that for some of the Hβ and Mg II profiles the single (or the second) Gaussian component was fitted to noise spikes or what appears to be a strong contribution from the narrow line region (judging from the strength of the [OIII] λ5007 line, when available) which gives the appearance of intrinsically very narrow broad-line profiles. For these profiles, the narrow component was discarded and the broad component alone, if available, was used to char-

acterize the profile. For profiles fitted with only a single Gaussian component, the emission line was discarded from further analysis. A total of 6 Hβ and 7 Mg II narrow profiles were discarded.

After this filtering of the data with the most uncertain measurements, we are left with measurements of a total of 139 Hβ, 654 Mg II, and 480 C IV profiles; a total of 134 quasars have measurements of both Hβ and Mg II, while 161 quasars have both Mg II and C IV measurements. Of the original 993 quasars analyzed by Forster et al. we were able to estimate the black hole masses for 978 quasars. The adopted FWHM values and the continuum luminosities used for the mass estimates are listed in Table 1. The black hole masses, bolometric luminosities, and Eddington luminosity ratios for the LBQS are listed in Table 2. Table 3 lists the basic properties (name, redshift, B_J magnitudes, and luminosity) of the LBQS quasars without mass estimates. The determination of the $M_{\rm BH}$ values are described in Section 3.

2.3. *The SDSS Color-selected Sample in the Fall Equatorial Stripe*

Fan et al. (2001a) present a well-defined color-selected sample of 38 quasars at $3.6 < z \leq 5.0$ from a 182 deg^2 field in the SDSS Fall Equatorial Stripe for which they determine the quasar luminosity function. The quasars were selected based on *gri* and *riz* colors to be complete in the survey area down to $i^* = 20$ mag. The continuum luminosities measured from the spectra were recalibrated to the dereddened AB(1450Å) magnitudes (see e.g., Vestergaard 2004a; see Fan et al. 2001a for details on these data). For four of the 38 quasars we are unable to obtain black hole mass estimates, because the (discovery) spectrum did not include the C IV emission line (J021043.17−001818.4, J021102.72−000910.3, J025019.78+004650.3) or the quality of the spectrum was too poor to measure FWHM(C IV) reasonably reliably (J020731.68+010348.9). For quasar J021102.72−000910.3 another spectrum is available in the SDSS archive, but we were unable to reliably measure spectral parameters for the mass estimate from that spectrum.

Fan et al. originally presented 39 quasars in this sample, but one source (J225529.09−003433.4) has since been reclassified as a star[3]; the spectrum is also missing from the discovery papers (Fan et al. 2001a; Schneider et al. 2001) and the SDSS Data Release 6 Archives.

This quasar sample was also included in the study by Vestergaard (2004a) on the distributions of black hole mass and Eddington luminosity ratios for distant quasars. Since improved mass estimation relations have been published more recently (Vestergaard & Peterson 2006), we redetermine the black hole masses for this sample. We adopt the measurements of FWHM(C IV) and 1350 Å continuum luminosities obtained and analyzed by Vestergaard (2004a).

The FWHM and continuum luminosity measurements used for the mass estimates of the SDSS color-selected sample are listed in Table 4. The black hole masses, bolometric luminosities, and Eddington luminosity ratios for these quasars are listed in Table 5. The computations

[3] This classification is verified by the NASA/IPAC Extragalactic Database (NED): http://nedwww.ipac.caltech.edu.

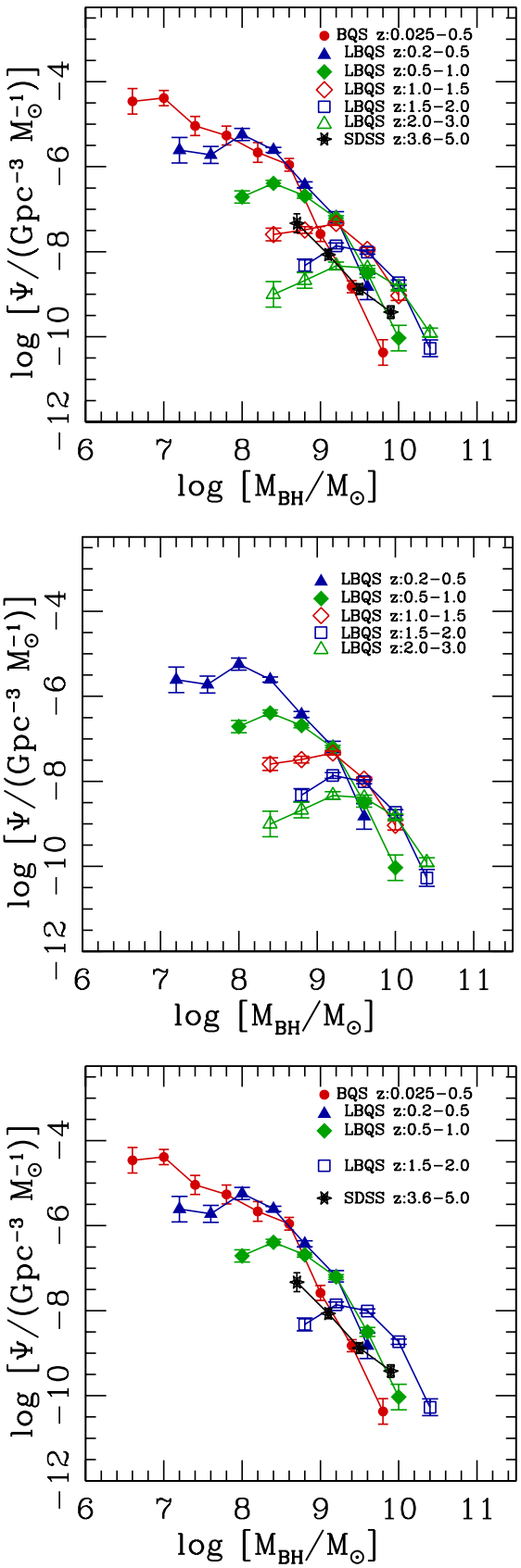

FIG. 4.— Mass functions as a function of mass for the samples analyzed in this work: *Top Panel*– the LBQS (for all five redshift bins), the BQS, and the SDSS color-selected samples; *Middle Panel* – the LBQS alone (for the five different redshift bins); *Lower Panel* – the BQS and the SDSS color-selected samples are shown with selected redshift bins of the LBQS for ease of comparison. The mass functions show turn-overs toward low masses due to incompleteness.

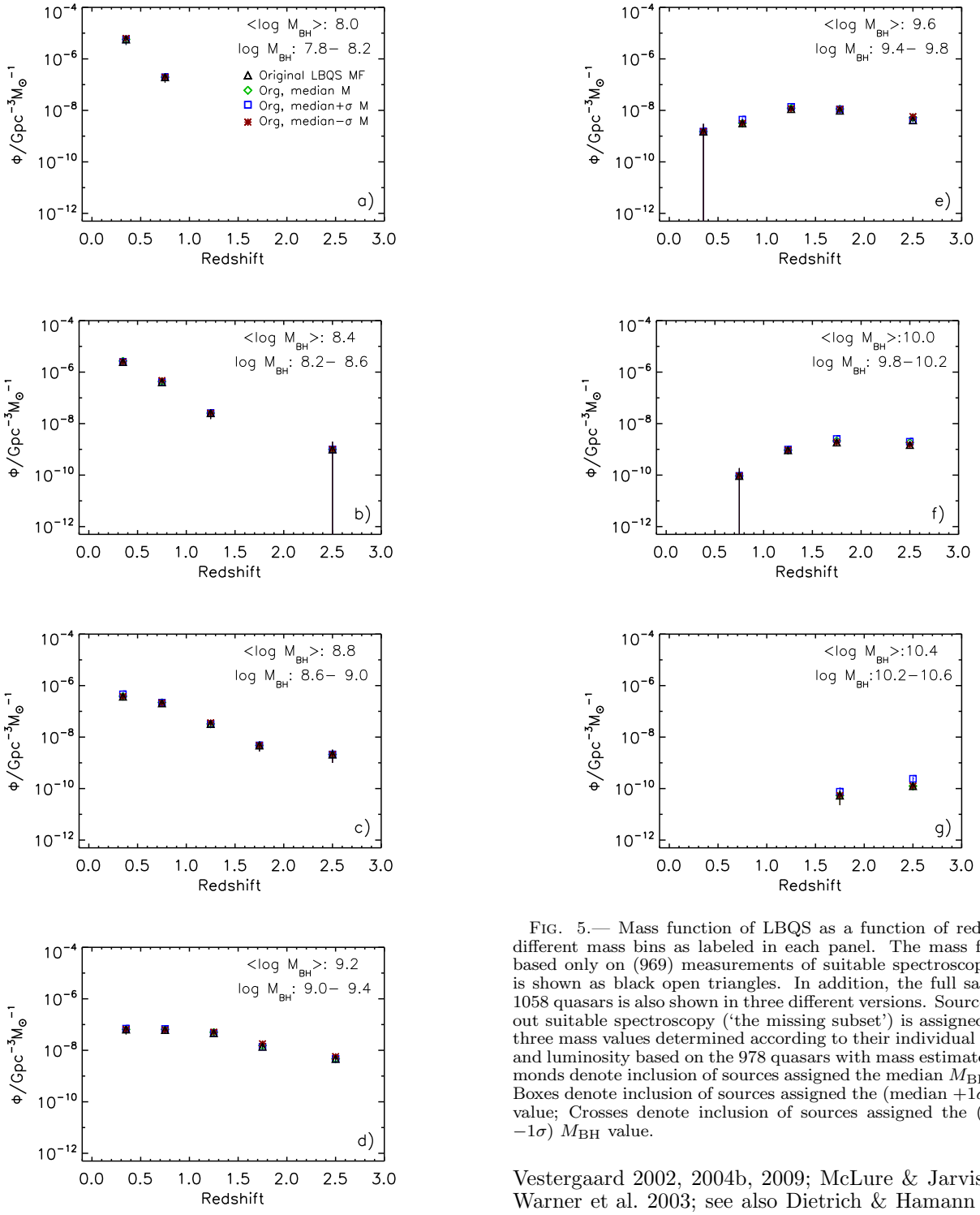

FIG. 5.— Mass function of LBQS as a function of redshift at different mass bins as labeled in each panel. The mass function based only on (969) measurements of suitable spectroscopic data is shown as black open triangles. In addition, the full sample of 1058 quasars is also shown in three different versions. Sources without suitable spectroscopy ('the missing subset') is assigned one of three mass values determined according to their individual redshift and luminosity based on the 978 quasars with mass estimates. Diamonds denote inclusion of sources assigned the median $M_{\rm BH}$ value; Boxes denote inclusion of sources assigned the (median $+1\sigma$) $M_{\rm BH}$ value; Crosses denote inclusion of sources assigned the (median -1σ) $M_{\rm BH}$ value.

FIG. 5.— ...figure is continued in next column...

are described in the next section.

3. BLACK HOLE MASS ESTIMATES

We determine black hole mass estimates using the so-called mass scaling relationships which utilize the widths of the broad emission lines and the nuclear continuum luminosities (e.g., Wandel, Peterson, & Malkan 1999; Vestergaard 2002, 2004b, 2009; McLure & Jarvis 2002; Warner et al. 2003; see also Dietrich & Hamann 2004). This method is preferred for several reasons (see also Vestergaard 2009). Only a couple of methods are applicable both to active galaxies in the nearby universe as well as the most distant quasars. Of these, mass scaling relationships have some of the lowest associated uncertainties (e.g., Vestergaard 2004b) which can be further improved upon in the future (e.g., Marconi et al. 2008). And quite importantly, these relationships are anchored in robust black hole mass determinations of low redshift active nuclei based on the reverberation mapping method (e.g., Blandford & McKee 1982; Peterson 1993) which have re-

cently been updated following a homogeneous reanalysis of the available reverberation database (Peterson et al. 2004; Onken et al. 2004). Moreover, the evidence in favor of our application of this method to more distant sources is quite strong (see e.g., Vestergaard 2004b, 2009, and references therein).

Black hole mass estimates can be obtained using one or more of the Hβ, Mg II, or C IV emission lines. For mass estimates based on Hβ and C IV we use equations (5) and (7), respectively, presented by Vestergaard & Peterson (2006); these relationships are calibrated to the most recently updated robust reverberation mapping mass determinations (Peterson et al. 2004; Onken et al. 2004). At present, there is no published relationship for the Mg II emission line which is (re)calibrated to the improved reverberation masses and also intercalibrated to the mass estimates based on the C IV emission line[4]. We therefore obtained a new relationship for Mg II using several thousand high-quality spectra from the SDSS DR3 quasar sample (Schneider et al. 2005). This relationship has been applied to the subset of the DR3 quasar sample used to establish the luminosity (Richards et al. 2006) and black hole mass (Vestergaard et al. 2008) functions. For completeness, we here present the relationships used. We obtained a relation for each of four monochromatic continuum luminosities because the 3000 Å luminosity may not always be accurately determined, sitting below the strong Fe II line emission at those wavelengths. We use the relation pertaining to the nuclear monochromatic continuum luminosity that can be best and most accurately measured in the observed spectrum. We refrain from extrapolating or adopting an assumed continuum slope in any of our work. For a given wavelength, λ, the black hole mass based on Mg II was obtained according to:

$$M_{\rm BH} = 10^{zp(\lambda)} \left[\frac{\rm FWHM(MgII)}{1000\,km/s}\right]^2 \left[\frac{\lambda L_\lambda}{10^{44}\,erg/s}\right]^{0.5} \quad (1)$$

where $zp(\lambda)$ is 6.72, 6.79, 6.86, and 6.96 for λ1350 Å, λ2100 Å, λ3000 Å, and λ5100 Å, respectively. The 1 σ scatter in the absolute zero-points, zp, is 0.55 dex which includes the factor $\sim$2.9 uncertainties of the reverberation mapping masses to which these mass estimation relations are anchored [see e.g., Vestergaard & Peterson (2006) and Onken et al. (2004) for details]. On average, these relations are consistent to within about 0.1 dex of the Hβ and C IV mass estimates. The relationships will be discussed further in a forthcoming paper (M. Vestergaard et al., in preparation).

A few of the BQS sources have been targeted by reverberation mapping. For those sources, we adopt the reverberation mass listed by Peterson et al. (2004). Since the objects in the BQS are all located at $z < 0.5$ we use the Hβ relationship to estimate the black hole mass for the remaining sources in this sample. Those mass estimates are listed in Table 7 of Vestergaard & Peterson (2006) and by Grier et al. (2008) for PG 2130+099.

The quasars in the LBQS span a large range of redshifts and therefore we applied all three emission line relations as follows. For any given source for which the FWHM of any of the three emission lines (Hβ, Mg II, C IV) could be reliably measured we determined an estimate of the mass based on each of these emission lines. If more than one emission line estimate is available for a given quasar, the final mass estimate of that source was determined as the weighted average of the available individual mass estimates. The adopted weights are the inverse variance determined from the propagated measurement errors. Therefore, for redshifts between 0.2 and 0.66 the mass estimate for each object is based on both the Hβ and Mg II emission lines while for redshifts between 1.04 and 1.71 the mass is based on both the Mg II and C IV lines. The black hole mass estimates for the LBQS are listed in Table 2.

The quasars in the SDSS color-selected sample all reside at redshifts for which only the C IV emission line can be observed using optical spectroscopy. We therefore use equation (7) of Vestergaard & Peterson (2006) to estimate the black hole masses for this sample. The mass values are tabulated in Table 5.

The distribution of (bolometric) luminosities and black hole masses with redshift is shown for all three samples in Figures 1 and 2, respectively. The bolometric luminosities, $L_{\rm bol}$, are obtained for the LBQS quasars by scaling monochromatic continuum luminosities at 1350 Å, 2100 Å, 3000 Å, and 5100 Å with a constant (average) bolometric correction factor[5] (of 4.3±0.46, 5.4±0.26, 5.8±0.24, and 10.5±0.24, respectively) extracted from Richards et al. (2006). For each quasar the $L_{\rm bol}$ value is determined from the monochromatic luminosity that is as closely centered in its optical observing window. For the SDSS color-selected sample, the 1350 Å continuum luminosity were similarly corrected for an estimate of the $L_{\rm bol}$ values. The BQS bolometric luminosities are adopted from Sanders et al. (1989) with appropriate cosmological corrections applied to conform to the cosmological model used in this work.

Figures 1 and 2 clearly demonstrate that since we can probe to lower luminosity limits in the nearby universe, we can also probe less massive black holes than at high redshift. While the BQS spans a large range in masses, it does not go very deep; recall, the limiting magnitude is $B_J \approx 16.2$ mag. The LBQS is also a 'bright' survey but has a lower flux limit (Fig. 1). This is also clear from the relative distributions of black hole masses at low redshifts for which there is some redshift overlap between the LBQS and the BQS (Fig. 2). The masses of the high-z color-selected sample and of the LBQS sources above a redshift of 1 are all of order a billion solar masses.

[4] The McGill et al. (2008) relations do not satisfy these requirements; they are based on a sample of only 19 SDSS quasars at $z \approx$0.36 and do not include a relation for C IV. We remind the reader that our ultimate intent is to compare and combine the mass functions presented here with those published by Vestergaard et al. (2008) on the SDSS DR3 quasar survey. For this particular purpose we need to use the *exact same* mass estimation relationships for all the individual mass functions.

[5] Note, the bolometric correction factors are suggested to depend on both black hole mass (Kelly et al. 2008b) and 'Eddington luminosity ratio' (Vasudevan & Fabian 2007) which may introduce systematic uncertainties in the derived $L_{\rm bol}/L_{\rm Edd}$ values in addition to those stemming from assuming a constant bolometric correction given that a range of spectral energy distributions exist of quasars (e.g., Elvis et al. 1994; Kuhn et al. 2001; Richards et al. 2006). Given that a robust adjustment scheme for the bolometric corrections has not been isolated and that the Eddington luminosity ratios are not analyzed further here, adopting a more complex correction factor is unnecessary at this time.

For completeness, we display the redshift distributions of the Eddington luminosity ratios, $L_{\rm bol}/L_{\rm Edd}$, in Figure 2. The quasars beyond $z \approx 1$ typically have $L_{\rm bol}/L_{\rm Edd}$ values between ∼0.1 and ∼1.0, while in the nearby universe the surveys can probe sources that accrete at rates down to about 1/100th of the Eddington limit. This distribution is consistent with earlier studies (e.g., Warner et al. 2003; Shemmer et al. 2004; McLure & Dunlop 2004; Vestergaard 2004; Kollmeier et al. 2006; Shen et al. 2008; Netzer & Traktenbrot 2007) and results showing that distant quasars are more actively accreting than local quasars and active nuclei (e.g., Peterson et al. 2004). It is important to keep in mind, here, that distant quasars also tend to be more luminous (e.g., Figure 1). Also, we show the distribution of FWHM of the emission lines with redshift in Figure 3. There is no significant change in FWHM with redshift with the exception that the SDSS quasars do not have the extreme wide lines that some LBQS quasars do.

4. BLACK HOLE MASS FUNCTIONS

The quasar black hole mass function, $\Psi(M_{\rm BH},z)$, is defined as the comoving space density of black holes per unit black hole mass as a function of black hole mass and redshift. To determine the space density (i.e., the number of black holes per unit comoving volume) in a given mass and redshift bin, we use the $1/V_a$ method presented by Warren, Hewett, & Osmer (1994), where V_a is the accessible volume, defined by Avni & Bahcall (1980). The mass function and its statistical uncertainty is described as

$$\Psi(< M_{\rm BH} >, < z >) = \sum_{i=1} \frac{1}{V_{a,i}\,\Delta M_{\rm BH}}, \quad \text{and} \quad (2)$$

$$\sigma(\Psi) = \left[\sum_{i=1} \left(\frac{1}{V_{a,i}\,\Delta M_{\rm BH}}\right)^2\right]^{1/2}, \quad (3)$$

respectively. The sum is performed over the objects (denoted by i) with redshift in the range $< z > -\Delta z/2$ and $< z > +\Delta z/2$ and with masses in the range $< M_{\rm BH} > -\Delta M_{\rm BH}/2$ and $< M_{\rm BH} > +\Delta M_{\rm BH}/2$.

We follow the method of Fan et al. (2001a) and Vestergaard et al. (2008) of including the selection function of the quasar survey in the computation of the accessible volume:

$$V_{a,i}\,(z_a) = \left(\int_{z_{\rm min}}^{z_a} p(z)\,\frac{dV}{dz}dz\right)_i \quad (4)$$

The "accessible redshift", z_a, is the minimum of $z_{\rm max}$, the maximum redshift that object i can have and still be detected by the survey, and the upper redshift limit in the survey or in the adopted redshift bin, i.e., $z_a = \min[z_{\rm max}, z_{\rm limit}]$. The volume element, dV/dz, is defined by Hogg (1999) for a ΛCDM cosmology.

For the BQS a constant survey completeness of p = 0.88, determined by Schmidt & Green (1983), was adopted. For the LBQS we adopt the survey completeness as a function of redshift presented by Hewett et al. (2001; their Table 7). The selection function for the SDSS color-selected sample was presented by Fan et al. (2001a) and is a function of both luminosity, redshift, and spectral energy distribution, $p(L, z, \text{SED})$.

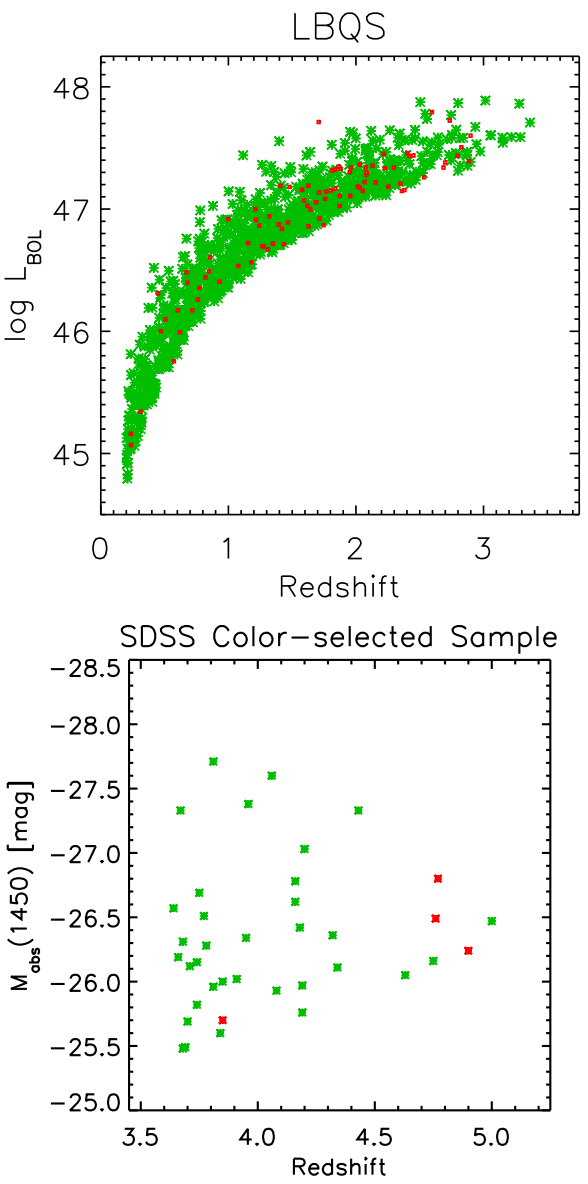

FIG. 6.— Distribution of luminosities with redshift of the LBQS (*Upper panel*) and SDSS color-selected (*Lower panel*) samples. The sources for which there are no spectroscopy available suitable for black hole mass estimates are highlighted.

We show the black hole mass functions of the three samples as a function of black hole mass in Figure 4. We limit the LBQS mass functions to redshifts below 3 since there are only nine quasars between redshifts 3 and 3.4; the LBQS mass functions are thus based on 969 quasars at $z \leq 3$. The LBQS sample is large enough to allow the mass functions to be determined for a range of redshift bins; they are shown in whole or in part in the various panels of Figure 4. This also allows us to display the mass functions as a function of redshift for a given black hole mass (Figure 5). The mass functions for the three quasar samples are tabulated in Tables 6, 7, and 9. Table 8 tabulates the redshift dependent mass function of the LBQS.

For 89 quasars (or about 8%) of the complete LBQS sample there is no spectral modeling available and therefore no black hole mass estimates exist for these sources.

We refer henceforth to this subset as the 'missing subset' (Figure 6). This affects the mass functions to some degree as we will underestimate the space density of certain black hole masses. In an attempt to estimate the most likely mass function for the entire LBQS sample we have used the observed distribution of black hole masses (for those quasars with reliable spectral modeling) to determine for each quasar in the missing subset the most likely black hole mass and the reasonably expected mass range around this value. From the observed distribution of LBQS black hole masses we determined the median mass and the standard deviation σ around this mass value in bins of z and B_J of widths $\Delta z = 0.1$ and $\Delta B_J = 0.5$; each bin has typically between 10 and 45 objects. For each of the 89 sources in the missing subset we used the observed redshift and B_J magnitude (see Fig. 6) to identify three mass values: the most likely mass (the median mass value of the observed distribution in the appropriate z and B_J bin) and the $\pm 1\sigma$ mass values relative thereto, respectively. We then generated three catalogs of 1058 black hole mass estimates at $z \leq 3$, each consisting of the original 969 black hole mass estimates based on spectral measurements plus for the missing subset either the most likely mass value, the most likely mass $+1\sigma(M_{\rm BH})$, or the most likely mass $-1\sigma(M_{\rm BH})$, respectively. For each of these three mass catalogs we redetermined the mass functions for LBQS. By adopting the same type of mass estimate for each quasar in the missing subset we get a handle on the most likely mass functions and the 1σ extremes. Notably, this is in practice different from running Monto Carlo simulations but gives us similar insight on the possible distributions of the mass functions. We show these adjusted mass functions as a function of mass in Figure 7. For comparison the mass functions based on only the 969 quasars (at $z \leq 3$) with spectral measurements (shown in Figure 4) are also shown. The adjusted mass functions are shown as a function of redshift in Figure 5. Our omission (or inclusion) of the missing subset clearly has no significant effect on the LBQS mass function.

Figure 7 shows that inclusion of the sources without mass estimates does not change the LBQS mass function (to within the statistical uncertainties) for redshifts below 2. At higher redshifts the missing sources will at one extreme ($M_{\rm BH}$(median) $-\sigma$) tend to increase the peak amplitude of the mass function slightly, and at the other extreme ($M_{\rm BH}$(median) $+\sigma$) the mass function will broaden slightly toward higher masses. The latter has the stronger effect due to the lower number of sources with mass estimates above $10^{10} M_{\odot}$. However, these variations are all within the statistical uncertainties with exception of the ($M_{\rm BH}$ $+\sigma$) mass function which is marginally more deviant. Notably, in reality the mass function of the full LBQS sample, that we could obtain if higher quality data were available of the missing subset, is more likely to be between the two extreme cases; as expected, assigning the median mass of the relevant z and B_J bin does not change the mass function. We therefore conclude that we are not making a significant error at this point in excluding the sources with low quality spectra (i.e., the missing subset) in determining the LBQS black hole mass function.

We repeated this exercise for the SDSS color-selected sample since for four of the 38 quasars the black hole mass could not be estimated. The effects of assigning $M_{\rm BH}$(median) $-\sigma(M_{\rm BH})$ or $M_{\rm BH}$(median) $+\sigma(M_{\rm BH})$ to these few sources are shown in Figure 8. The differences in the mass functions are most noticeable when the extreme mass values of $M_{\rm BH}$(median) $+\sigma$ are adopted: the mass function flattens slightly toward higher mass values. Nonetheless, this extreme case mass function is still consistent to within the statistical uncertainties with the "original" mass function based on the 34 quasars with spectral measurements (i.e., Figure 4). Therefore, exclusion of the four sources without mass estimates does not significantly affect the mass function of the SDSS color-selected sample.

We will reassess this issue of missing black hole masses in future work when analyzing the mass functions from this work with respect to the SDSS DR3 mass functions of Vestergaard et al. (2008).

The black hole mass functions for the LBQS and the SDSS color-selected samples with these adjustments applied are listed in Tables 10 and 9, respectively.

5. CUMULATIVE MASS DENSITIES

The integrated mass density above a certain mass value in each sample is computed by summing the contribution of each individual object with central mass above a progressively increasing mass limit, M_k:

$$\rho\,(\geq M_k) = \int_{M_k}^{\rm inf} \frac{M_{\rm BH,i}}{V_{a,i}} \qquad (5)$$

Figure 9 shows the cumulative mass densities for each of the SDSS, BQS, and LBQS samples. The mass densities are tabulated in Table 11 for the SDSS and BQS samples and in Tables 7 and 10 for the LBQS.

In Figure 10 we show the distributions of $\Psi \cdot M_{\rm BH}$ for comparison. This representation is closer to the comoving volume (number) density of active black holes as a function of mass and makes the space density differences more apparent.

6. DISCUSSION

The mass functions for the three quasar samples are shown as a function of black hole mass for different redshift bins in Figure 4. Three features are apparent: (1) the mass functions of the LBQS tend to turn over at the low mass end, (2) there is a general consistency of the slope of the high mass end between the mass functions in most of the redshift bins, and (3) the amplitude of the high mass end increases rapidly between mean redshifts of 4 to 2.5 and then decrease again below a redshift of 1. This is particularly significant for the cumulative mass density (Fig. 9). We briefly comment on each feature in the following.

The turnover at the low mass end tends to occur when the low mass bins are incompletely populated [cf. with Fig. 2; see also the discussion of the SDSS DR3 mass functions by Vestergaard et al. (2008) and the statistical analysis of Kelly, Vestergaard, & Fan (2009)]. However, the analysis of the BQS mass function by Kelly et al. indicates that part of such turnovers (at least at low redshift) are real, suggesting that the number of low mass active black holes does not necessarily stay constant or increase with decreasing mass.

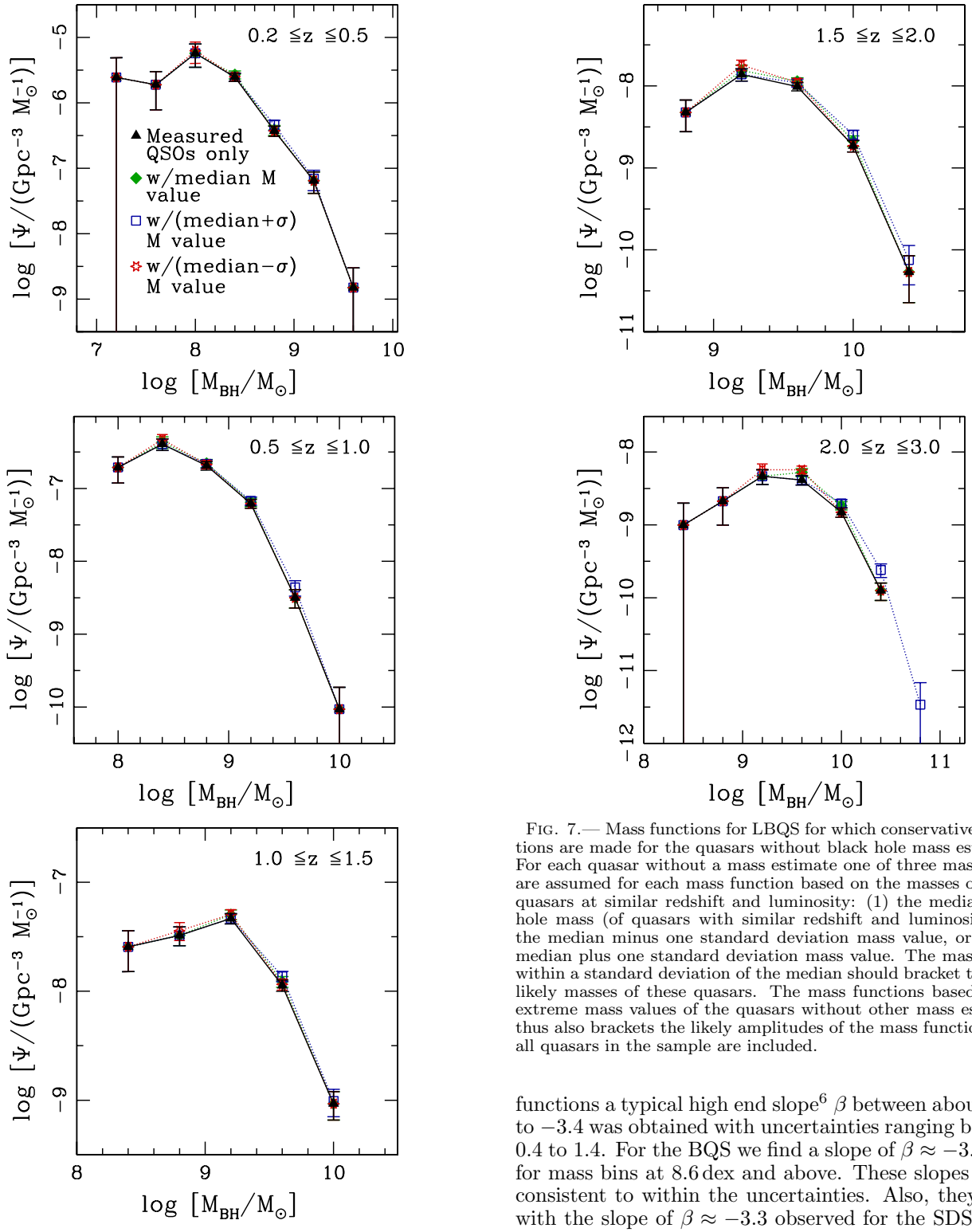

FIG. 7.— Mass functions for LBQS for which conservative corrections are made for the quasars without black hole mass estimates. For each quasar without a mass estimate one of three mass values are assumed for each mass function based on the masses of LBQS quasars at similar redshift and luminosity: (1) the median black hole mass (of quasars with similar redshift and luminosity), (2) the median minus one standard deviation mass value, or (3) the median plus one standard deviation mass value. The mass values within a standard deviation of the median should bracket the most likely masses of these quasars. The mass functions based on the extreme mass values of the quasars without other mass estimates thus also brackets the likely amplitudes of the mass function when all quasars in the sample are included.

FIG. 7.— continued in next column

We determine the high mass end slopes, β, of each mass function in Fig. 4 (*top panel*) following the method of Vestergaard et al. (2008) where $\Psi \propto M^{\beta}$. We first discuss the mass functions located at redshifts below 3.5 and thereafter discuss the case at $z \geq 3.5$. For the LBQS mass functions a typical high end slope[6] β between about -3.0 to -3.4 was obtained with uncertainties ranging between 0.4 to 1.4. For the BQS we find a slope of $\beta \approx -3.6 \pm 1.0$ for mass bins at 8.6 dex and above. These slopes are all consistent to within the uncertainties. Also, they agree with the slope of $\beta \approx -3.3$ observed for the SDSS DR3 mass function below redshifts of about 3.8 (Vestergaard et al. 2008). It is interesting to note that the high-end slopes of the SDSS DR3 luminosity functions also have

[6] Specifically, slopes of $-3.0, -3.4, -2.7, -2.9, -2.6$ were obtained for the redshift bins [0.2:0.5], [0.5:1.0], [1.0:1.5], [1.5:2.0], and [2.0:3.0], respectively, for mass bins at or above 8.8 dex, 9.2 dex, 9.6 dex, 9.6 dex, and 10.0 dex, respectively. The limits on the mass bins were adopted to ensure the mass bins are complete or nearly complete. Note that given the uncertainties of between 0.4 to 1.4 there are no reasons to believe the apparent flattening of the mass functions toward higher redshifts is real.

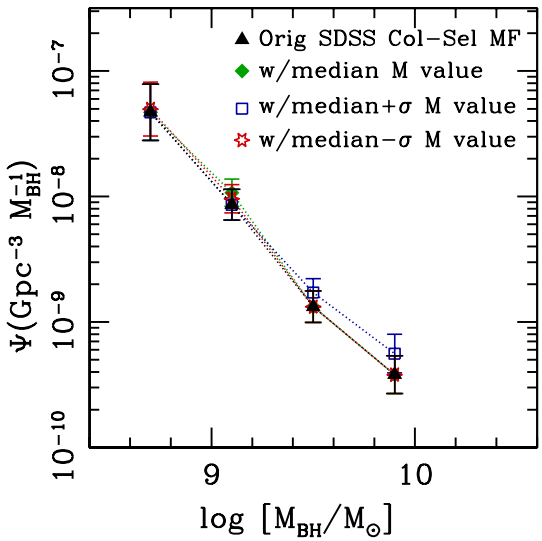

FIG. 8.— Mass function for the SDSS color-selected sample for which conservative corrections are made for the quasars without black hole mass estimates. For each quasar without a mass estimate one of three mass values are assumed for each mass function based on the masses of quasars at similar redshift: (1) the median black hole mass of quasars with similar redshift, (2) the median minus one standard deviation mass value, or (3) the median plus one standard deviation mass value.

values of $\beta \approx -3.3$ (Richards et al. 2006).

However, for the mass function above redshift 3.5, i.e., of the SDSS color-selected sample, we see a somewhat flatter slope of $\beta \approx -1.75 \pm 0.56$, determined for mass bins at 8.6 dex and above. The reality of this flatter slope is also evident from Figure 4. Vestergaard et al. also reported an apparent flattening of the DR3 mass function slopes at $z \gtrsim 4$ but attributed this to the large errors and small number statistics in those redshift bins. Since the color-selected sample is a well-defined and complete sample within the survey area and flux limits, the result for this sample should be robust, suggesting that there is indeed a real trend toward the high-mass black hole distribution to flatten at the highest redshifts.

The constancy of the high mass end slope and of the amplitude of the mass function with redshift (at $z \lesssim 3$) may appear surprising, especially considering the large changes occurring for the evolution of the luminosity function (e.g., Boyle et al. 2000; Richards et al. 2006). For example, the amplitude of the SDSS DR3 luminosity function drops more than two orders of magnitude at an absolute magnitude of -27 between redshifts two and 0.5. In comparison, the DR3 black hole mass function normalization changes only by a factor of a few and displays a similar constancy of the high mass end slope and amplitude at a wide range of redshifts. While this slope constancy may be real, we note the possibility that the statistical uncertainties in the black hole mass estimates of a factor of a few prohibits us from detecting subtle differences or any cosmic evolution of the high mass end slope. One issue to keep in mind is that contrary to the quasar luminosity, the mass of black holes does not decrease with time. The only way for the black holes to change the shape of the mass functions with cosmic time is by growing in mass or by their activity to decrease sufficiently to drop out of the quasar survey owing to its lower flux limits.

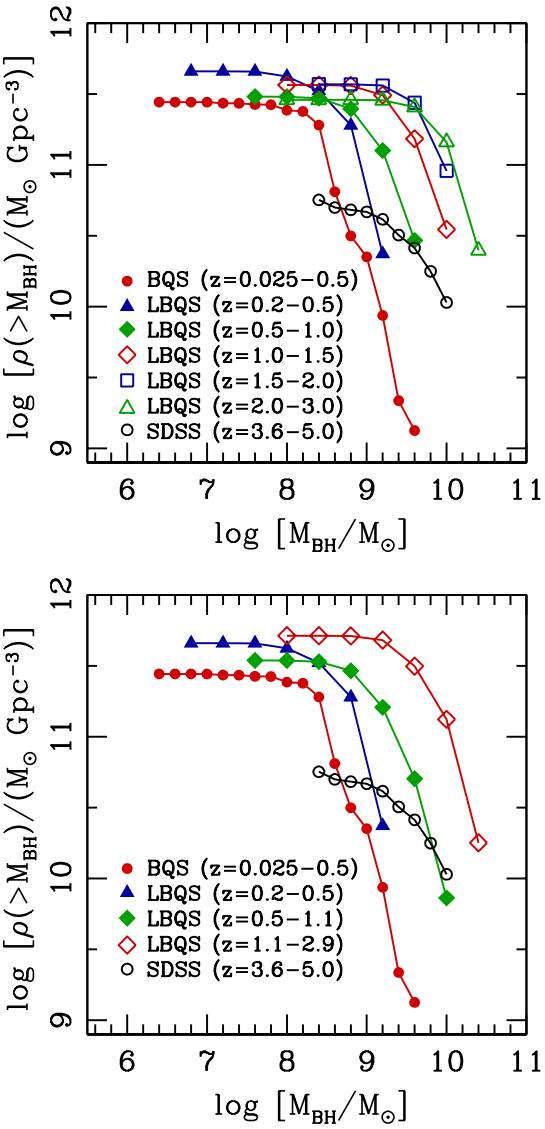

FIG. 9.— Cumulative mass density of active supermassive black holes for different redshift bins of the LBQS and for the BQS and SDSS color-selected samples as a function of black hole mass. The top panel shows the BQS and SDSS color-selected samples with the five redshift bins of the LBQS as are also shown in Figure 4. The lower panel displays fewer redshift bins for LBQS for a different, less cluttered view.

The mass function and the cumulative mass density distribution both display a rapid increase in amplitude at the highest masses by a factor of ∼5 and ∼10, respectively, over a period of a Giga-year from redshifts 4 (SDSS) to 2.5 (LBQS, $2 \leq z \leq 3$). This is an interesting feature, especially considering the slower amplitude decrease below $z \approx 1$; it is even more evident in the particular representation of the mass function shown in Figure 10. We are evidently directly seeing the population of massive black holes build up at these epochs as the density of actively accreting (massive) black holes rises rapidly toward lower redshift. This is also consistent with the observed rise in the quasar space density at these redshifts (e.g., Osmer 1982; Schmidt et al. 1995; Warren et al. 1994; Fan et al. 2001b) and the relatively high Eddington luminosity ratios observed for the SDSS color-selected sample (Fig. 2).

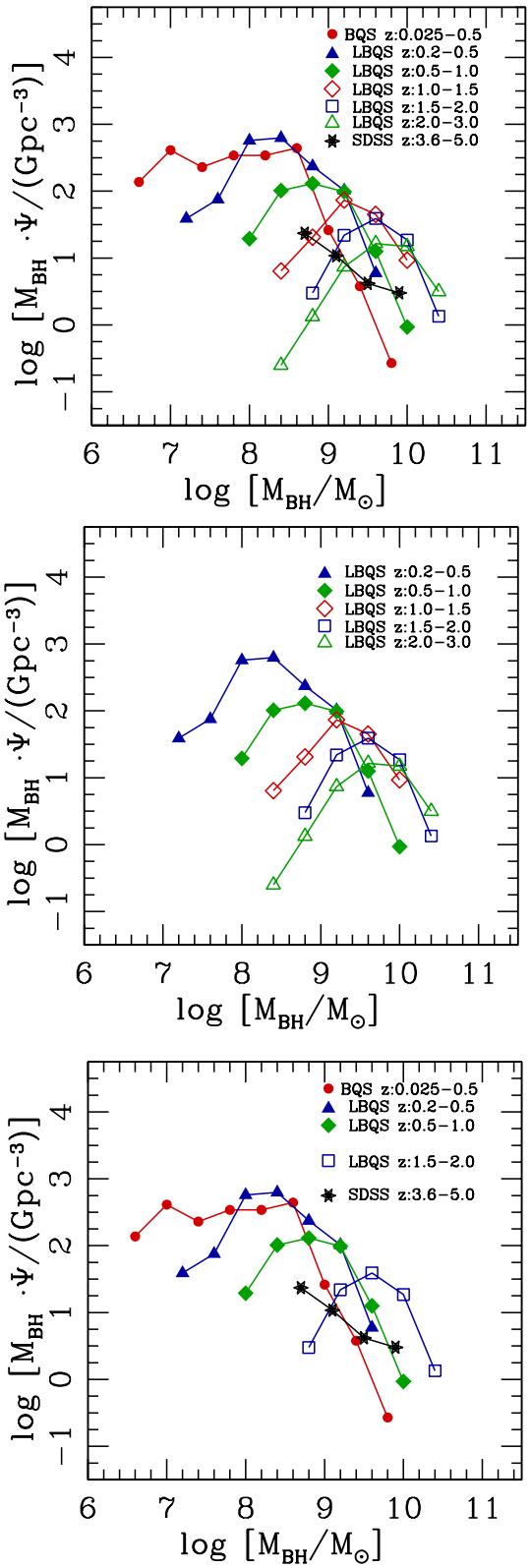

FIG. 10.— Distributions of $\Psi \cdot M_{\rm BH}$ as a function of black hole mass; Ψ is the black hole mass function. *Top Panel*– the LBQS (for all five redshift bins), the BQS, and the SDSS color-selected samples; *Middle Panel* – the LBQS alone (for the five different redshift bins); *Lower Panel* – the BQS and the SDSS color-selected samples are shown with selected redshift bins of the LBQS for ease of comparison.

We note that the space density information revealed by the luminosity functions does not make the mass functions obsolete. The luminosity functions tell us the space density of active black holes radiating at a given luminosity and redshift. The luminosity itself tells us how fast the black hole is accreting matter given the efficiency by which it converts matter to radiation but does not reveal whether we are observing a highly accreting, low mass black hole or a massive black hole accreting at moderate or low rates. The mass estimates confirm the latter scenario. The dashed line in Fig. 2 (top panel) shows the SDSS flux limits folded with the cut-off in line widths of 1000 km s^{-1} adopted for the SDSS quasars (Schneider et al. 2003). If the former scenario was reality we would see the data points accumulate on and just above this dashed line. Instead, we see a much wider distribution well above this limit. This is an important fact to keep in mind. The mass estimates and the mass functions also serve to break the degeneracy of the luminosity functions due to the loosely constrained radiative efficiency (e.g., Wyithe & Radmanabhan 2006), as noted in the introduction.

The distinctly lower amplitudes of the mass function and the cumulative mass density distribution for the SDSS sample at redshift four (Fig. 4) show that there are somewhat fewer active black holes at a given mass and/or less massive active black holes at that epoch than at later cosmic times. In particular, high-z quasars contribute very little to the mass density of active black holes. To examine this a little further and to test if this is merely a consequence of our inability to detect very low mass black holes at $z \approx 4$, we extrapolated the SDSS mass function to very low masses based on the observed slope at the lower mass end ($\lesssim 10^9\,M_\odot$). This extrapolation is shown in the top panel of Figure 11 (dashed line), allowing a comparison with the mass functions of the BQS and LBQS samples. We also show with a dotted line the general slope along which the LBQS mass functions at redshifts lower than two move with cosmic time. It is quite conceivable that, in the case of no survey flux limits, the LBQS mass functions would extend approximately along this line, since the SDSS DR3 mass functions (Vestergaard et al. 2008) exhibit a similar behavior. The dotted line is hence a guideline to the maximum growth that can occur from the earliest epochs according to observations. The extrapolated mass function at $z \approx 4$ is clearly parallel to the dotted line, offset by about $0.6 - 0.65$ dex in mass and about 1.25 dex in space density. This parallel offset suggests that the SDSS quasars are either rarer than at lower epochs by a factor of $\sim$17 or they need to grow in mass by an average factor of 4 to 4.5 by redshift 2.5 (ignoring black hole mergers). Given the time passed between redshifts of four and 2.5 (of order 1 Gyr) and quasar life times of much less than a Giga year (e.g., Martini 2004; Hopkins & Hernquist 2008), the massive black holes that are contributing to the mass function at $z \approx 4$ are not the same most massive black holes observed at $z \approx 2.5$. The most massive black holes at $z \approx 4$ would have ceased their activity and dropped out of our surveys by $z \approx 2.5$. Hence, the shift in the mass functions at the highest masses is not due to simple mass growth and a space density increase must dominate. Since galaxy mergers (and hence black hole mergers) are expected to occur more frequently in the

earlier universe than at present, we expect that the less massive black holes (than typically observed at redshift four) undergo a combination of both minor and major mergers as well as growth by mass accretion between the epochs at redshifts four and two. This will cause these black holes to shift to higher masses and the mass function amplitude at the high mass end to shift upwards.

In the lower panel of Figure 11 we show the cumulative mass density for the SDSS extrapolated mass function. Unless the distribution of low-mass black holes is significantly steeper than the extrapolated power-law discussed here then it is clear that the lack of detectable low-mass black holes at $z \approx 4$ is not the reason for the large amplitude discrepancies (both panels) between the quasar populations observed at very early ($z \approx 4$) and at later ($z < 2$) epochs. A significant build-up of existing and future supermassive black holes is required to explain the quasar populations at later times.

We therefore conclude that the active black hole population at high redshift must be different since significantly fewer active black holes exist and with lower mass density at $z \approx 4$ than at $z \approx 2.5$ and $z \approx 0.5$, respectively. An interesting theoretical exercise would be to place lower limits on the distribution of 'seed' (i.e., low mass) black holes at redshifts of four required to explain the local distribution of (lower mass) black holes ($M_{\rm BH} \lesssim 10^8 M_\odot$) for later observational tests of this prediction, for example, similar to the work by Volonteri et al. (2008).

When comparing all the samples at redshifts below three the high-mass end of the mass functions show little mass growth in these black holes. In fact, the density of the highest mass black holes decreases with cosmic time at epochs later than $z \approx 1$, consistent with a general decrease in activity of the most massive black holes. This is also and more clearly seen in the representation of the mass function shown for different mass bins as a function of redshift, as we discuss next. Although the LBQS only has about 1000 quasars distributed over a range of redshifts, it is still large enough to allow a determination of how the mass function depends on redshift for a given mass bin (Fig. 5). (The value of the LBQS in this regard will become particularly apparent when discussed in relation to the mass function of the SDSS DR3 quasar sample which is statistically limited near a redshift of 3.) This representation of the mass function directly shows at which epochs active black holes at a given mass are the most abundant. For example, the black holes of lower masses of $7.8 - 8.6$ dex peak in their comoving space density in the local universe, while the more massive black hole of 10^{10} $M_\odot$ are the most active at redshifts of $2 - 3$. Figure 5f shows that the expected density of such black holes is more than two orders of magnitude lower in the local universe. By comparing the mass functions for individual mass bins the cosmic downsizing (e.g., Ueda et al. 2003) of active black holes is clearly evident: the most massive black holes are the most active at high redshifts while the lowest mass black holes are the most active at low redshift.

7. SUMMARY

We present the mass functions of actively accreting black holes for the Bright Quasar Survey, the Large Bright Quasar Survey, and the SDSS color-selected sample in the Fall Equatorial Stripe and the database from

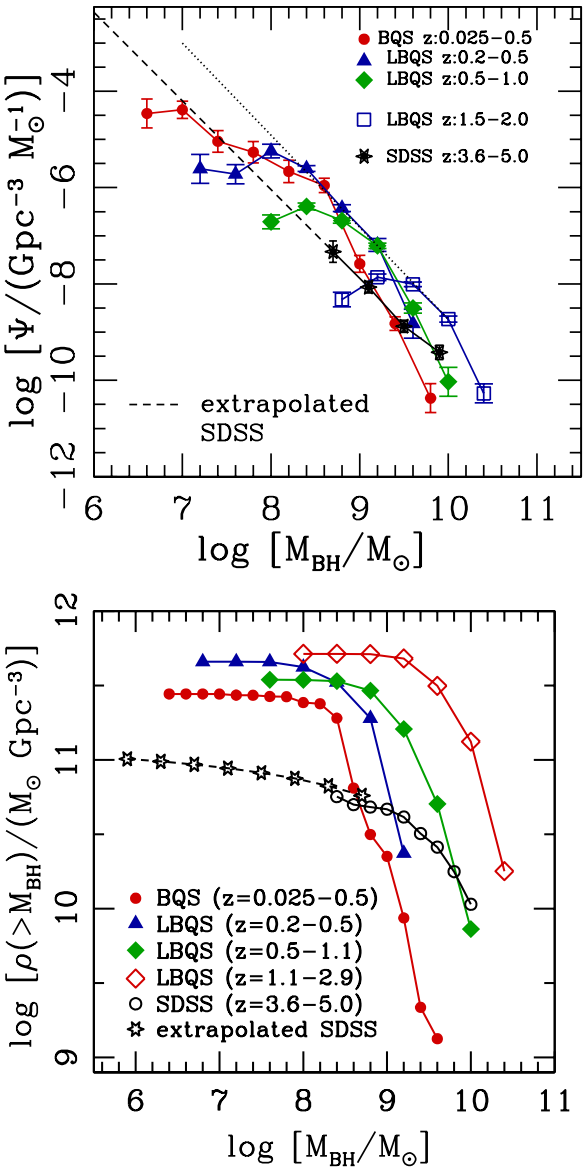

FIG. 11.— Mass functions (top panel) and cumulative mass densities (lower panel) as a function of black hole mass. These diagrams show the same distributions as Figure 4 (bottom panel) and Figure 9 (lower panel) with an extrapolation applied to the SDSS distributions. In the top panel the SDSS mass function is extrapolated (dashed line) to very low mass values based on the observed slope of the mass function. This extrapolated mass function is used to compute the resulting cumulative mass density for that sample, assuming we had no flux limits. The extrapolated cumulative mass density is overplotted in the lower panel on the previously introduced mass densities from Figure 9. The dotted line in the top panel is a guideline to the maximum growth in the black holes that the observations allow (see section 6 for discussion).

which these mass functions are derived. We find similar amplitudes and slopes (of about $\beta \approx -3.3$ with uncertainties between 0.4 and 1.4) of the high mass end of the mass functions for different redshift bins and across quasar samples for redshifts below ~3.5. This is similar to what was seen for the DR3 mass functions at a similar redshift range (Vestergaard et al. 2008). However, for the well-defined and complete SDSS color-selected sample of quasars at redshifts between 3.6 and 5 we find a somewhat flatter slope of $\beta = -1.75 \pm 0.56$. Comparison of the mass functions and the cumulative mass density

distributions for the different samples shows that the active black hole population at redshifts of about 4 must be different than the black hole populations below a redshift of about 2.5. In fact, we may be witnessing a fast build-up of the black hole population between redshifts of 4 and redshifts of ∼2.

The mass functions presented here will be discussed in further detail in relation to other existing black hole mass functions and, in particular, the SDSS DR3 mass functions (Vestergaard et al. 2008) in a future paper (M. Vestergaard et al. 2009, in preparation). At that time we will also apply sophisticated statistical analysis (Kelly et al. 2008a, 2009) to investigate the nature of the actual underlying mass distribution free of measurement uncertainties and, to a certain extent, of survey flux limits.

We thank Dave Sanders for providing his tabulation of observed bolometric luminosities of the BQS sample, Xiaohui Fan for comments on the manuscript, and Brandon Kelly for discussions. MV thanks for their hospitality the astronomy departments at the Ohio State University and the University of Arizona where most of this work was performed. We gratefully acknowledge financial support through HST grants HST-AR-10691, HST-GO-10417, and HST-GO-10833 from NASA through the Space Telescope Science Institute, which is operated by the Association of Universities for Research in Astronomy, Inc., under NASA contract NAS5-26555.

facilities: HST (FOS,STIS), KPNO: 2.1m (Gold), SDSS, MMT (blue channel spectrograph), Keck: I (LRIS), UKST (direct, objective prism).

REFERENCES

Avni, Y., & Bahcall, J. N. 1980, ApJ, 235, 694
Blandford, R. D., & McKee, C. F. 1982, ApJ, 255, 419
Boyle, B. J., Shanks, T., Croom, S. M., Smith, R. J., Miller, L., Loaring, N., & Heymans, C. 2000, MNRAS, 317, 1014
Boroson, T. & Green, R. 1992, ApJ, 80, 109
Brotherton, M. S. 1996, ApJS, 102, 1
Collin, S., Kawaguchi, T., Peterson, B.M., Vestergaard, M. 2006, A&A, 456, 75
Crampton, D., Cowley, A. P., & Hartwick, F. D. A. 1987, ApJ, 314, 129
Denney, K., Peterson, B.M., Dietrich, M., Vestergaard, M., Bentz, M.C. 2009, ApJ, 692, 246
Dietrich, M. & Hamann, F. 2004, ApJ, 611, 761
Fan, X. 2006, New Astronomy Review, 50, 665
Fan, X., et al. 2001a, AJ, 121, 31
Fan, X., et al. 2001b, AJ, 122, 2833
Ferrarese, L. 2003, Hubble's Science Legacy: Future Optical/Ultraviolet Astronomy from Space, 291, 196
Foltz, C. B., Chaffee, F. H., Jr., Hewett, P. C., MacAlpine, G. M., Turnshek, D. A., Weymann, R. J., & Anderson, S. F. 1987, AJ, 94, 1423
Forster, K., Green, P.J., Aldcroft, T.L., Vestergaard, M., Foltz, C.B., & Hewett, P.C., 2001, ApJS, 134, 35
Granato, G. L., De Zotti, G., Silva, L., Bressan, A., & Danese, L. 2004, ApJ, 600, 580
Grier, C. J., et al. 2008, ApJ, 688, 837
Green, R. F., Schmidt, M., & Liebert, J. 1986, ApJS, 61, 305
Hewett, P. C., Foltz, C. B., & Chaffee, F. H. 1995, AJ, 109, 1498
Hewett, P.C., Foltz, C.B., Chaffee, F.H. 2001, AJ, 122, 518
Huchra, J., & Burg, R. 1992, ApJ, 393, 90
Hogg, D. W. 1999, ArXiv Astrophysics e-prints, arXiv:astro-ph/9905116
Hopkins, P. F., & Hernquist, L. 2008, arXiv:0809.3789
Jester, S., et al. 2005, AJ, 130, 873
Kelly, B. C., Fan, X., & Vestergaard, M. 2008a, ApJ, 682, 874
Kelly, B. C., Bechtold, J., Trump, J. R., Vestergaard, M., & Siemiginowska, A. 2008b, ApJS, 176, 355
Kelly, B., Vestergaard, M., & Fan, X. 2009, ApJ, 692, 1388
Kibblewhite, E. J., Bridgeland, M. T., Bunclark, P. S., & Irwin, M. J. 1984, Astronomical Microdensitometry Conference, 277
Kollmeier, J. A., et al. 2006, ApJ, 648, 128
Koo, D. C., & Kron, R. G. 1982, A&A, 105, 107
Krolik, J. H. 2001, ApJ, 551, 72
Kuhn, O., Elvis, M., Bechtold, J., & Elston, R. 2001, ApJS, 136, 225
Magorrian, J., et al. 1998, AJ, 115, 2285
Marconi, A., Axon, D. J., Maiolino, R., Nagao, T., Pastorini, G., Pietrini, P., Robinson, A., & Torricelli, G. 2008, ApJ, 678, 693
McLure, R. J., & Dunlop, J. S. 2004, MNRAS, 352, 1390
McLure, R. J., & Jarvis, M. J. 2002, MNRAS, 337, 109
McNamara, B. R., & Nulsen, P. E. J. 2007, ARA&A, 45, 117
Martini, P. 2004, Coevolution of Black Holes and Galaxies, 169
Morris, S. L., Weymann, R. J., Anderson, S. F., Hewett, P. C., Francis, P. J., Foltz, C. B., Chaffee, F. H., & MacAlpine, G. M. 1991, AJ, 102, 1627
Netzer, H., & Trakhtenbrot, B. 2007, ApJ, 654, 754
Onken, C.A., et al. 2004, ApJ, 615, 645
Osmer, P. S. 1982, ApJ, 253, 28
Peterson, B.M., 1993, PASP, 105, 247
Peterson, B.M. et al. 2004, ApJ, 613, 682
Richards, G. T., et al. 2006, AJ, 131, 2766
Richards, G. T., Vanden Berk, D. E., Reichard, T. A., Hall, P. B., Schneider, D. P., SubbaRao, M., Thakar, A. R., & York, D. G. 2002, AJ, 124, 1
Sanders, D. B., Phinney, E. S., Neugebauer, G., Soifer, B. T., Matthews, K. 1989, ApJ, 347, 29
Shen, Y., Greene, J. E., Strauss, M. A., Richards, G. T., & Schneider, D. P. 2008, ApJ, 680, 169
Shemmer, O., et al. 2004, ApJ, 614, 547
Schlegel, D. J., Finkbeiner, D. P., & Davis, M. 1998, ApJ, 500, 525
Schneider, D. et al. 2001, AJ, 130, 367
Schneider, D. et al 2003, AJ, 126, 2579
Schneider, D. et al. 2005, AJ, 130, 367
Schmidt, M., & Green, R. F. 1983, ApJ, 269, 352
Schmidt, M., Schneider, D. P., & Gunn, J. E. 1995, AJ, 110, 68
Smith, R. J., Croom, S. M., Boyle, B. J., Shanks, T., Miller, L., & Loaring, N. S. 2005, MNRAS, 359, 57
Somerville, R. S., Hopkins, P. F., Cox, T. J., Robertson, B. E., & Hernquist, L. 2008, MNRAS, 391, 481
Springel, V., Di Matteo, T., & Hernquist, L. 2005, MNRAS, 361, 776
Tremaine, S., et al. 2002, ApJ, 574, 740
Ueda, Y., Akiyama, M., Ohta, K., & Miyaji, T. 2003, ApJ, 598, 886
Véron-Cetty, M.-P., Joly, M., & Véron, P. 2004, A&A, 417, 515
Vestergaard, M. 2002, ApJ, 571, 733
Vestergaard, M. 2004a, ApJ, 601, 676
Vestergaard, M. 2004b, in AGN Physics with the Sloan Digital Sky Survey, ApJ, ASP Conference Series, 311, 69
Vestergaard, M. 2009, in the STScI Spring Symposium 2007 on 'Black Holes', ed. A. Koekemoer, Cambridge University Press, in press (astro-ph: arXiv:0904.2615)
Vestergaard, M., & Peterson, B. M. 2006, ApJ, 641, 689
Vestergaard, M., Fan, X., Tremonti, C. A., Osmer, P. O., Richards, G. T. 2008, ApJ, 674, L1
Vestergaard, M., & Wilkes, B. J. 2001, ApJS, 134, 1
Vestergaard, M., Wilkes, B. J., & Barthel, P. D. 2000, ApJ, 538, L103
Volonteri, M., Lodato, G., & Natarajan, P. 2008, MNRAS, 383, 1079
Wandel, A., Peterson, B.M., Malkan, M. 1999, ApJ, 526, 579
Warner, C., Hamann, F., & Dietrich, M. 2003, ApJ, 596, 72
Warren, S. J., Hewett, P. C., & Osmer, P. S. 1994, ApJ, 421, 412
Wills, B., Browne, I. 1986, ApJ, 302, 56
Wyithe, J. S. B., & Padmanabhan, T. 2006, MNRAS, 372, 1681
York, D. G., et al. 2000, AJ, 120, 1579

TABLE 1
Line Widths and Nuclear Luminosities of the LBQS quasars.

Name (1)	z (2)	FWHM(Hβ) (km s^{-1}) (3)	FWHM(Mg II) (km s^{-1}) (4)	FWHM(C IV) (km s^{-1}) (5)	log[$L_{\lambda 1350}$ /erg s^{-1}] (6)	log[$L_{\lambda 2100}$ /erg s^{-1}] (7)	log[$L_{\lambda 3000}$ /erg s^{-1}] (8)	log[$L_{\lambda 5100}$ /erg s^{-1}] (9)
Q0000+0159	1.073	···	4000^{+500}_{-450}	···	$42.81^{+0.18}_{-0.31}$	$42.52^{+0.25}_{-0.62}$	$42.29^{+0.32}_{-42.29}$	$41.94^{+0.45}_{-41.94}$
Q0001−0050	1.459	···	4000^{+400}_{-400}	5000^{+350}_{-325}	$42.98^{+0.20}_{-0.39}$	$42.69^{+0.28}_{-0.98}$	$42.46^{+0.36}_{-42.46}$	$42.11^{+0.50}_{-42.11}$
Q0002−0243	0.432	3200^{+325}_{-300}	3111^{+92}_{-124}	···	$41.99^{+0.14}_{-0.20}$	$41.70^{+0.19}_{-0.34}$	$41.47^{+0.24}_{-0.61}$	$41.12^{+0.35}_{-41.12}$

Note. — FWHM measurements are based on Forster et al. (2001) and the luminosities are computed from the B_J survey magnitudes (Hewett et al. 2001, and references therein). For cases where the relative luminosity error exceed 1.0 the negative error of the logarithm of the luminosity cannot be computed and this error is instead assigned the value of the luminosity itself. This Table is listed in its entirety in the online journal. Only sample entries are listed here.

TABLE 2
LBQS Black Hole Mass Estimates and Luminosities

Name (1)	z (2)	B_J (3)	log[$M_{\rm BH}/M_\odot$] (4)	log[$L_{\rm bol}$/erg s^{-1}] (5)	log $L_{\rm bol}/L_{\rm Edd}$ (6)
Q0000+0159	1.073	18.43	$8.92^{+0.16}_{-0.26}$	$46.57^{+0.26}_{-0.71}$	$-0.441^{+0.284}_{-0.120}$
Q0001−0050	1.459	18.74	$9.13^{+0.18}_{-0.18}$	$46.74^{+0.29}_{-1.17}$	$-0.483^{+0.315}_{-0.127}$
Q0002−0243	0.432	18.27	$8.32^{+0.23}_{-0.23}$	$45.71^{+0.25}_{-0.68}$	$-0.713^{+0.311}_{-0.953}$

Note. — This Table is listed in its entirety in the online journal. Only sample entries are listed here.

TABLE 3
Basic Properties of LBQS Sources without Black Hole Mass Estimates

Name (1)	z (2)	B_J (3)	log[$L_{\rm bol}$/erg s^{-1}] (4)
Q0004+0147	1.710	18.13	47.14
Q0010−0012	2.154	18.46	47.22
Q0013−0029	2.083	18.18	47.30
Q0018+0047	1.835	17.82	47.32
Q0018−0220	2.596	17.44	47.79

Note. — This Table is listed in its entirety in the online journal. Only sample entries are listed here.

TABLE 4
Line Widths and Nuclear Luminosities of the SDSS Color-selected quasars.

Name (1)	z (2)	$p^{\rm a}$ (3)	FWHM(C IV) (km s^{-1}) (4)	log[$L_{\lambda 1350}$ /erg s^{-1}] (5)
J001950.06−004040.9	4.32	0.90	4706^{+1396}_{-539}	$43.436^{+0.020}_{-0.020}$
J003525.29+004002.8	4.75	0.99	2150^{+150}_{-100}	$43.366^{+0.031}_{-0.033}$
J005922.65+000301.4	4.16	0.78	3325^{+425}_{-175}	$43.536^{+0.012}_{-0.012}$

Note. — FWHM and luminosity measurements are adopted from Vestergaard (2004a). This Table is listed in its entirety in the online journal. Only sample entries are listed here.
[a] Selection probability (Fan et al. 2001)

TABLE 5
SDSS Color−selected Sample Black Hole Mass Estimates and Luminosities

Name (1)	z (2)	$\log[M_{\rm BH}/M_\odot]$ (3)	$\log[L_{\rm bol}/{\rm erg\ s^{-1}}]$ (4)	$\log\ L_{\rm bol}/L_{\rm Edd}$ (5)
J001950.06−004040.9	4.32	$9.345^{+0.360}_{-0.771}$	$47.230^{+0.048}_{-0.054}$	$-0.2146^{+0.3602}_{-0.7742}$
J003525.29+004002.8	4.75	$8.627^{+0.333}_{-0.823}$	$47.160^{+0.053}_{-0.060}$	$0.4330^{+0.3339}_{-0.8320}$
J005922.65+000301.4	4.16	$9.096^{+0.338}_{-0.817}$	$47.330^{+0.046}_{-0.051}$	$0.1342^{+0.3376}_{-0.8187}$

Note. — This Table is listed in its entirety in the online journal. Only sample entries are listed here.

TABLE 6
BQS Black Hole Mass Function

$< z >$ (1)	Δz[a] (2)	$< M_{\rm BH} >$[b] ($M_\odot$) (3)	$\Psi(M,z)$ (Gpc$^{-3}M_\odot{}^{-1}$) (4)	$\sigma(\Psi)$ (Gpc$^{-3}M_\odot{}^{-1}$) (5)	N (6)
0.25	0.25	6.6	3.448E-05	3.448E-05	1
		7.0	4.112E-05	2.108E-05	6
		7.4	9.114E-06	6.162E-06	7
		7.8	5.419E-06	3.634E-06	11
		8.2	2.165E-06	1.529E-06	17
		8.6	1.107E-06	4.501E-07	22
		9.0	2.619E-08	1.297E-08	13
		9.4	1.506E-09	5.765E-10	9
		9.8	4.235E-11	4.235E-11	1

[a] The range of the redshift bin is $< z > \pm\Delta z$.[b] The central mass in the bin. The mass bin size is 0.4 dex and expands ±0.2 dex relative to the central mass value.

TABLE 7
LBQS Black Hole Mass Function

$< z >$ (1)	Δz[a] (2)	$< M_{\rm BH} >$[b] ($M_\odot$) (3)	$\Psi(M,z)$ (Gpc$^{-3}M_\odot{}^{-1}$) (4)	$\sigma(\Psi)$ (Gpc$^{-3}M_\odot{}^{-1}$) (5)	N (6)	$\rho(> M_{\rm BH})$[c] ($M_\odot$Mpc^{-3}) (7)
0.35	0.15	6.8	···	···	0	461.03
0.35	0.15	7.2	2.4518E-06	2.4518E-06	1	460.50
0.35	0.15	7.6	1.8975E-06	1.1120E-06	5	459.29
0.35	0.15	8.0	5.7041E-06	2.2265E-06	26	423.53
0.35	0.15	8.4	2.4266E-06	3.5559E-07	75	335.24
0.35	0.15	8.8	3.7082E-07	6.5793E-08	39	196.06
0.35	0.15	9.2	6.5978E-08	2.3601E-08	15	37.805
0.35	0.15	9.6	1.5007E-09	1.5007E-09	1	···
0.75	0.25	7.6	···	···	0	322.67
0.75	0.25	8.0	1.9470E-07	7.6028E-08	9	322.07
0.75	0.25	8.4	4.0175E-07	7.4011E-08	54	315.12
0.75	0.25	8.8	2.0598E-07	2.7534E-08	90	268.67
0.75	0.25	9.2	6.0881E-08	8.4790E-09	77	145.79
0.75	0.25	9.6	3.1654E-09	8.8983E-10	13	51.704
0.75	0.25	10.0	3.6235E-10	1.8121E-10	4	8.9008
1.25	0.25	7.6	···	···	0	394.74
1.25	0.25	8.0	5.3376E-09	5.3376E-09	1	394.70
1.25	0.25	8.4	2.5527E-08	1.0412E-08	7	394.38
1.25	0.25	8.8	3.0814E-08	6.2483E-09	27	391.50
1.25	0.25	9.2	4.5757E-08	5.0341E-09	105	338.64
1.25	0.25	9.6	1.0996E-08	1.3039E-09	76	182.61
1.25	0.25	10.0	1.2521E-09	3.0845E-10	20	63.610
1.25	0.25	10.4	2.1249E-11	2.1249E-11	1	···
1.75	0.25	8.4	···	···	0	374.11
1.75	0.25	8.8	4.7534E-09	1.9897E-09	6	373.94
1.75	0.25	9.2	1.3410E-08	2.3147E-09	38	367.59
1.75	0.25	9.6	9.5608E-09	1.1030E-09	79	282.15
1.75	0.25	10.0	1.9367E-09	3.0588E-10	41	98.379
1.75	0.25	10.4	5.3655E-11	3.0978E-11	3	···
2.50	0.50	8.0	···	···	0	291.62
2.50	0.50	8.4	9.9367E-10	9.9367E-10	1	291.62
2.50	0.50	8.8	2.1144E-09	1.1199E-09	4	291.21
2.50	0.50	9.2	4.5198E-09	1.0667E-09	24	289.26
2.50	0.50	9.6	4.1379E-09	6.0390E-10	55	259.84
2.50	0.50	10.0	1.4573E-09	2.1311E-10	52	150.49
2.50	0.50	10.4	1.3643E-10	3.5502E-11	15	24.924

[a] The range of the redshift bin is $< z > \pm \Delta z$.[b] The central mass in the bin. The mass bin size is 0.4 dex and expands ± 0.2 dex relative to the central mass value.[c] The lower mass limit is the central value of the mass bin listed in column 3.

TABLE 8
The LBQS Redshift Dependent Black Hole Mass Function

$< M_{\rm BH} >$[a] ($M_\odot$) (1)	$< z >$ (2)	Δz[b] (3)	$\Psi(M,z)$ (Gpc$^{-3}M_\odot{}^{-1}$) (4)	$\sigma(\Psi)$ (Gpc$^{-3}M_\odot{}^{-1}$) (5)	N (6)
8.00	0.35	0.15	5.7292E-06	2.2287E-06	25
8.00	0.75	0.25	1.9470E-07	7.6028E-08	9
8.00	1.25	0.25	···	···	0
8.00	1.75	0.25	···	···	0
8.00	2.50	0.50	···	···	0
8.40	0.35	0.15	2.4872E-06	3.5733E-07	78
8.40	0.75	0.25	4.0640E-07	7.4157E-08	55
8.40	1.25	0.25	2.5527E-08	1.0412E-08	7
8.40	1.75	0.25	···	···	0
8.40	2.50	0.50	9.9367E-10	9.9367E-10	1
8.80	0.35	0.15	3.7392E-07	6.6183E-08	40
8.80	0.75	0.25	2.0598E-07	2.7534E-08	90
8.80	1.25	0.25	3.2505E-08	6.3618E-09	29
8.80	1.75	0.25	4.7534E-09	1.9897E-09	6
8.80	2.50	0.50	2.1144E-09	1.1199E-09	4
9.20	0.35	0.15	6.4744E-08	2.3427E-08	15
9.20	0.75	0.25	6.2003E-08	8.5161E-09	79
9.20	1.25	0.25	4.6456E-08	5.0355E-09	108
9.20	1.75	0.25	1.3817E-08	2.3514E-09	39
9.20	2.50	0.50	4.6557E-09	1.0753E-09	25
9.60	0.35	0.15	1.5007E-09	1.5007E-09	1
9.60	0.75	0.25	3.1654E-09	8.8983E-10	13
9.60	1.25	0.25	1.1309E-08	1.3366E-09	77
9.60	1.75	0.25	9.8252E-09	1.1188E-09	81
9.60	2.50	0.50	4.1379E-09	6.0390E-10	55
10.00	0.35	0.15	···	···	0
10.00	0.75	0.25	9.3214E-11	9.3214E-11	1
10.00	1.25	0.25	9.2919E-10	2.7036E-10	15
10.00	1.75	0.25	1.8614E-09	2.9647E-10	40
10.00	2.50	0.50	1.4888E-09	2.1542E-10	53
10.40	0.35	0.15	···	···	0
10.40	0.75	0.25	···	···	0
10.40	1.25	0.25	···	···	0
10.40	1.75	0.25	5.3655E-11	3.0978E-11	3
10.40	2.50	0.50	1.2549E-10	3.3775E-11	14

[a] The central mass in the bin. The mass bin size is 0.4 dex and expands $\pm$0.2 dex relative to the central mass value.[b] The range of the redshift bin is $< z > \pm \Delta z$.

TABLE 9
Black Hole Mass Function of the SDSS Color-selected Sample

$< z >$	Δz[a]	$< M_{\rm BH} >$[b] ($M_\odot$)	$\Psi(M,z)$ (Gpc$^{-3}M_\odot{}^{-1}$)	$\sigma(\Psi)$ (Gpc$^{-3}M_\odot{}^{-1}$)	N
(1)	(2)	(3)	(4)	(5)	(6)
Measured $M_{\rm BH}$ Values Only (Original Mass Function)					
4.3	0.7	8.7	4.690E-08	3.162E-08	6
4.3	0.7	9.1	8.607E-09	2.800E-09	13
4.3	0.7	9.5	1.325E-09	4.462E-10	9
4.3	0.7	9.9	3.798E-10	1.569E-10	6
Measured $M_{\rm BH}$ and Assigned Median $M_{\rm BH}$ Values					
4.3	0.7	8.7	4.690E-08	3.162E-08	6
4.3	0.7	9.1	1.072E-08	3.073E-09	17
4.3	0.7	9.5	1.325E-09	4.462E-10	9
4.3	0.7	9.9	3.798E-10	1.569E-10	6
Measured $M_{\rm BH}$ and Assigned Median $M_{\rm BH}+1\sigma$ Values					
4.3	0.7	8.7	4.690E-08	3.162E-08	6
4.3	0.7	9.1	8.607E-09	2.800E-09	13
4.3	0.7	9.5	1.715E-09	4.997E-10	12
4.3	0.7	9.9	5.597E-10	2.386E-10	7
Measured $M_{\rm BH}$ and Assigned Median $M_{\rm BH}-1\sigma$ Values					
4.3	0.7	8.7	4.975E-08	3.175E-08	7
4.3	0.7	9.1	9.585E-09	2.856E-09	16
4.3	0.7	9.5	1.325E-09	4.462E-10	9
4.3	0.7	9.9	3.798E-10	1.569E-10	6

[a] The range of the redshift bin is $< z > \pm\Delta z$.[b] The central mass in the bin. The mass bin size is 0.4 dex and expands $\pm$0.2 dex relative to the central mass value.

TABLE 10
Corrected LBQS Black Hole Mass Function

$< z >$ (1)	Δz[a] (2)	$< M_{\rm BH} >$[b] ($M_\odot$) (3)	$\Psi(M,z)$ (Gpc$^{-3}M_\odot{}^{-1}$) (4)	$\sigma(\Psi)$ (Gpc$^{-3}M_\odot{}^{-1}$) (5)	N (6)	$\rho(> M_{\rm BH})$[c] ($M_\odot$Mpc^{-3}) (7)
Measured $M_{\rm BH}$ and Assigned Median $M_{\rm BH}$ Values						
0.35	0.15	6.8	···	···	0	475.05
0.35	0.15	7.2	2.4518E-06	2.4518E-06	1	474.52
0.35	0.15	7.6	1.8975E-06	1.1120E-06	5	473.31
0.35	0.15	8.0	5.7292E-06	2.2287E-06	25	437.86
0.35	0.15	8.4	2.7017E-06	3.7761E-07	82	345.18
0.35	0.15	8.8	3.8550E-07	6.7189E-08	41	190.48
0.35	0.15	9.2	6.4744E-08	2.3427E-08	15	23.53
0.35	0.15	9.6	1.5007E-09	1.5007E-09	1	···
0.75	0.25	7.6	···	···	0	318.57
0.75	0.25	8.0	1.9470E-07	7.6028E-08	9	317.97
0.75	0.25	8.4	4.3218E-07	7.8509E-08	56	311.02
0.75	0.25	8.8	2.2154E-07	2.8136E-08	98	259.42
0.75	0.25	9.2	6.5052E-08	8.6269E-09	84	130.77
0.75	0.25	9.6	3.1654E-09	8.8983E-10	13	29.34
0.75	0.25	10.0	9.3214E-11	9.3214E-11	1	···
1.25	0.25	8.000	···	···	0	389.25
1.25	0.25	8.400	2.5527E-08	1.0412E-08	7	388.93
1.25	0.25	8.800	3.2505E-08	6.3618E-09	29	385.78
1.25	0.25	9.200	5.0448E-08	5.2050E-09	118	332.50
1.25	0.25	9.600	1.2247E-08	1.3828E-09	84	157.13
1.25	0.25	10.000	9.2919E-10	2.7036E-10	15	35.06
1.75	0.25	8.400	···	···	0	420.21
1.75	0.25	8.800	4.7534E-09	1.9897E-09	6	420.04
1.75	0.25	9.200	1.5414E-08	2.4894E-09	43	412.79
1.75	0.25	9.600	1.1405E-08	1.1958E-09	95	313.36
1.75	0.25	10.000	2.1402E-09	3.1767E-10	46	90.84
1.75	0.25	10.400	5.3655E-11	3.0978E-11	3	···
2.50	0.50	8.000	···	···	0	338.39
2.50	0.50	8.400	9.9367E-10	9.9367E-10	1	338.39
2.50	0.50	8.800	2.1144E-09	1.1199E-09	4	337.98
2.50	0.50	9.200	4.6557E-09	1.0753E-09	25	336.03
2.50	0.50	9.600	5.2545E-09	6.7097E-10	71	306.28
2.50	0.50	10.000	1.8430E-09	2.3892E-10	66	147.96
2.50	0.50	10.400	1.2549E-10	3.3775E-11	14	24.92
Measured $M_{\rm BH}$ and Assigned Median $M_{\rm BH}+1\sigma$ Values						
0.35	0.15	6.8	···	···	0	502.79
0.35	0.15	7.2	2.4518E-06	2.4518E-06	1	502.25
0.35	0.15	7.6	1.8975E-06	1.1120E-06	5	501.05
0.35	0.15	8.0	5.7292E-06	2.2287E-06	25	465.59
0.35	0.15	8.4	2.4872E-06	3.5733E-07	78	377.61
0.35	0.15	8.8	4.5933E-07	8.2115E-08	44	224.05
0.35	0.15	9.2	6.9354E-08	2.3876E-08	16	35.714
0.35	0.15	9.6	1.5007E-09	1.5007E-09	1	···
0.75	0.25	7.6	···	···	0	335.75
0.75	0.25	8.0	1.9470E-07	7.6028E-08	9	335.15
0.75	0.25	8.4	4.0640E-07	7.4157E-08	55	328.20
0.75	0.25	8.8	2.1765E-07	2.9418E-08	92	281.43
0.75	0.25	9.2	6.7637E-08	8.8044E-09	86	146.66
0.75	0.25	9.6	4.3793E-09	1.0455E-09	18	32.929
0.75	0.25	10.0	9.3214E-11	9.3214E-11	1	···
1.25	0.25	8.0	···	···	0	409.27
1.25	0.25	8.4	2.5527E-08	1.0412E-08	7	408.95
1.25	0.25	8.8	3.2505E-08	6.3618E-09	29	405.79
1.25	0.25	9.2	4.6456E-08	5.0355E-09	108	353.76
1.25	0.25	9.6	1.3702E-08	1.4729E-09	93	176.43
1.25	0.25	10.0	9.8256E-10	2.7558E-10	16	35.057
1.75	0.25	8.4	···	···	0	473.23
1.75	0.25	8.8	4.7534E-09	1.9897E-09	6	473.06
1.75	0.25	9.2	1.3817E-08	2.3514E-09	39	465.81
1.75	0.25	9.6	1.0912E-08	1.1868E-09	89	376.75
1.75	0.25	10.0	2.5353E-09	3.4376E-10	55	162.89
1.75	0.25	10.4	7.5198E-11	3.7732E-11	4	14.133
2.50	0.50	8.0	···	···	0	402.11
2.50	0.50	8.4	9.9367E-10	9.9367E-10	1	402.11
2.50	0.50	8.8	2.1144E-09	1.1199E-09	4	401.69
2.50	0.50	9.2	4.6557E-09	1.0753E-09	25	399.74
2.50	0.50	9.6	4.1379E-09	6.0390E-10	55	369.99
2.50	0.50	10.0	1.9763E-09	2.4675E-10	71	255.72
2.50	0.50	10.4	2.4082E-10	5.1114E-11	24	34.871

TABLE 10 — *Continued*

$< z >$ (1)	Δz[a] (2)	$< M_{\rm BH} >$[b] ($M_\odot$) (3)	$\Psi(M,z)$ (Gpc$^{-3}M_\odot{}^{-1}$) (4)	$\sigma(\Psi)$ (Gpc$^{-3}M_\odot{}^{-1}$) (5)	N (6)	$\rho(> M_{\rm BH})$[c] ($M_\odot$Mpc^{-3}) (7)
2.50	0.50	10.8	3.4121E-12	3.4121E-12	1	···
Measured $M_{\rm BH}$ and Assigned Median $M_{\rm BH}$ -1σ Values						
0.35	0.15	6.8	···	···	0	464.72
0.35	0.15	7.2	2.4518E-06	2.4518E-06	1	464.19
0.35	0.15	7.6	1.8975E-06	1.1120E-06	5	462.98
0.35	0.15	8.0	6.2681E-06	2.2497E-06	29	427.52
0.35	0.15	8.4	2.5162E-06	3.5851E-07	79	333.11
0.35	0.15	8.8	3.7392E-07	6.6183E-08	40	190.48
0.35	0.15	9.2	6.4744E-08	2.3427E-08	15	23.53
0.35	0.15	9.6	1.5007E-09	1.5007E-09	1	···
0.75	0.25	7.6	···	···	0	310.60
0.75	0.25	8.0	1.9470E-07	7.6028E-08	9	310.00
0.75	0.25	8.4	4.7127E-07	7.9844E-08	64	301.02
0.75	0.25	8.8	2.1364E-07	2.7751E-08	95	252.17
0.75	0.25	9.2	6.2003E-08	8.5161E-09	79	126.47
0.75	0.25	9.6	3.1654E-09	8.8983E-10	13	29.34
0.75	0.25	10.0	9.3214E-11	9.3214E-11	1	···
1.25	0.25	8.0	···	···	0	378.83
1.25	0.25	8.4	2.5527E-08	1.0412E-08	7	378.52
1.25	0.25	8.8	3.5906E-08	6.6951E-09	32	374.77
1.25	0.25	9.2	5.0778E-08	5.1932E-09	120	315.32
1.25	0.25	9.6	1.1577E-08	1.3500E-09	79	153.21
1.25	0.25	10.0	9.2919E-10	2.7036E-10	15	35.06
1.75	0.25	8.4	···	···	0	395.31
1.75	0.25	8.8	4.7534E-09	1.9897E-09	6	395.14
1.75	0.25	9.2	1.7965E-08	2.6306E-09	52	385.18
1.75	0.25	9.6	1.1090E-08	1.1821E-09	92	274.61
1.75	0.25	10.0	1.8614E-09	2.9647E-10	40	90.84
1.75	0.25	10.4	5.3655E-11	3.0978E-11	3	···
2.50	0.50	8.0	···	···	0	310.87
2.50	0.50	8.4	9.9367E-10	9.9367E-10	1	310.87
2.50	0.50	8.8	2.1144E-09	1.1199E-09	4	310.45
2.50	0.50	9.2	5.7111E-09	1.1510E-09	32	308.50
2.50	0.50	9.6	5.7243E-09	7.0062E-10	77	257.20
2.50	0.50	10.0	1.4888E-09	2.1542E-10	53	144.92
2.50	0.50	10.4	1.2549E-10	3.3775E-11	14	24.92

[a] The range of the redshift bin is $< z > \pm \Delta z$.[b] The central mass in the bin. The mass bin size is 0.4 dex and expands ± 0.2 dex relative to the central mass value.[c] The lower mass limit is the central value of the mass bin listed in column 3.

TABLE 11
Cumulative Mass Densities of the BQS and SDSS Color-selected Samples

	BQS	**SDSS Color-selected Sample**			
$< M_{\rm BH} >^{a}$ ($M_\odot$) (1)	$\rho(> M_{\rm BH})^{b}$ ($M_\odot {\rm Mpc}^{-3}$) (2)	$\rho(> M_{\rm BH})^{b,c}$ ($M_\odot {\rm Mpc}^{-3}$) (3)	$\rho_{\rm corr,Med}(> M_{\rm BH})^{b,d}$ ($M_\odot {\rm Mpc}^{-3}$) (4)	$\rho_{\rm corr,Med+\sigma}(> M_{\rm BH})^{b,e}$ ($M_\odot {\rm Mpc}^{-3}$) (5)	$\rho_{\rm corr,Med-\sigma}(> M_{\rm BH})^{b.f}$ ($M_\odot {\rm Mpc}^{-3}$) (6)
6.4	278.2	···	···	···	···
6.6	277.8	···	···	···	···
6.8	277.8	···	···	···	···
7.0	277.5	···	···	···	···
7.2	272.9	···	···	···	···
7.4	272.3	···	···	···	···
7.6	267.4	···	···	···	···
7.8	265.8	···	···	···	···
8.0	243.3	···	···	···	···
8.2	238.9	···	···	···	···
8.4	190.8	56.56	61.07	67.89	58.41
8.6	64.72	49.96	54.46	61.29	51.80
8.8	31.52	48.25	52.76	59.58	50.09
9.0	22.43	46.69	51.20	58.02	46.69
9.2	8.656	41.33	45.84	52.67	41.33
9.4	2.168	31.99	31.99	43.32	31.99
9.6	1.334	25.95	25.95	33.10	25.95
9.8	···	17.73	17.73	17.73	17.73
10.0	···	10.69	10.69	10.69	10.69

[a] The central mass in the bin. The mass bin size is 0.4 dex and expands ±0.2 dex relative to the central mass value.[b] The lower mass limit is the central value of the mass bin listed in column 1.[c] Cumulative mass density for the original mass function based on measured spectral measurements only.[d] Cumulative mass density for the full sample based on measured spectral measurements and assigned mass values (median $M_{\rm BH}$) for sources without a suitable spectrum.[e] Cumulative mass density for the full sample based on measured spectral measurements and assigned mass values (median $M_{\rm BH}$ $+1\sigma$) for sources without a suitable spectrum.[f] Cumulative mass density for the full sample based on measured spectral measurements and assigned mass values (median $M_{\rm BH}$ -1σ) for sources without a suitable spectrum.